Synthesis of Prussian Blue nanoparticles in water/alcohol mixtures

Pavel Khramtsov[a,b,*], Maria Kropaneva[a,b], Dmitriy Kiselkov[c,d], Artem Minin[e,f], Larisa Chekanova[c], Mikhail Rayev[a,b].

[a] Institute of Ecology and Genetics of Microorganisms, Urals Branch of RAS, Perm, 614081, Russia

[b] Biology faculty, Perm State University, Perm, 614990, Russia

[c] Institute of Technical Chemistry, Urals Branch of RAS, Perm, 614068, Russia;

[d] Perm National Research Polytechnic University, Perm, 614990, Russia

[e] M.N. Mikheev Institute of Metal Physics Urals Branch of RAS, Ekaterinburg, 620108, Russia

[f] Ural Federal University, Ekaterinburg, 620002, Russia

* Corresponding author: E-mail: khramtsovpavel@yandex.ru; phone: +7 (342) 280 77 94

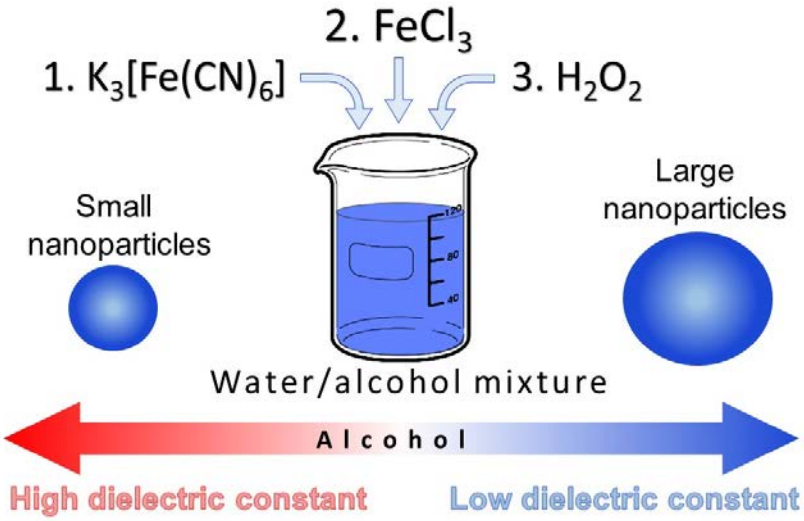

Abstract

Prussian Blue, a blue coordination polymer, emerges as a promising candidate in the realm of biomedicine. Its nanoparticles, known as catalytic labels or nanozymes, exhibit remarkable peroxidase-like properties and serve as effective antioxidants. Unsurprisingly, the demand

for synthesizing Prussian Blue nanoparticles with customizable sizes is on the rise. In this study, we unveil a novel approach to synthesizing Prussian Blue nanoparticles. In this work, the synthesis of Prussian Blue nanoparticles by reducing an equimolar mixture of $FeCl_3$ and $K_3[Fe(CN)_6]$ with hydrogen peroxide in different water-alcohol mixtures was demonstrated for the first time. Alcohols with a lower dielectric constant (propanol-1, isopropyl alcohol, and tert-butanol) contribute to an increase in nanoparticle size, particularly at mole fractions of 0.02-0.05 and beyond. Conversely, alcohols with a higher dielectric constant (ethanol, methanol, ethylene glycol, and propylene glycol, excluding glycerol) demonstrate the ability to decrease nanoparticle size at mole fractions of 0.2-0.26 and higher. Building upon these findings, we present a scalable and reproducible method for preparing small Prussian Blue nanoparticles, measuring 30-40 nm, with enhanced peroxidase-like activity using 79.2% ethylene glycol as a solvent. The proposed mechanism behind the effect of ethylene glycol involves the limitation of both growth and secondary aggregation of Prussian Blue nanoparticles. These synthesized nanoparticles prove their efficiency as catalytic labels in a model vertical flow immunoassay designed to detect antibodies against SARS-CoV-2.

Keywords

Coordination polymer, polyol synthesis, co-precipitation, nanozyme

Highlights

- Prussian Blue nanoparticles were synthesized in water-alcohol mixtures
- The size of the nanoparticles depended on the fraction and dielectric constant of the alcohol
- A scalable and reproducible method was demonstrated for synthesizing small (30-40 nm) nanoparticles

1. Introduction

Prussian Blue, an iron-based blue pigment with a rich history dating back to the 18th century [1], has found widespread use in coloring paints, inks, plastics, textiles, and other materials. In the medical field, Prussian Blue, marketed as Radiogardase, is prescribed for oral treatment of radioactive cesium or thallium contamination. The bright color and metal

cation absorption capabilities of Prussian Blue stem from its unique cage-like structure, composed Fe^{3+} and Fe^{2+} atoms bridged by C≡N groups [2,3].

In recent years, Prussian Blue nanoparticles have emerged as promising mimetics of the iron-containing enzyme, horseradish peroxidase, finding applications in colorimetric assays and electrochemical sensors [4]. Horseradish peroxidase catalyzes the oxidation of colorless substrate molecules to colored products using hydrogen peroxide as a second substrate. This property has made horseradish peroxidase a popular choice as a label in enzyme-linked immunosorbent assays (ELISA), a fundamental tool in modern clinical diagnosis. Despite the high efficiency of horseradish peroxidase, there have been numerous attempts to replace the enzyme with more catalytically active and stable mimics. Various metal nanoparticles, including noble metal nanoparticles, perovskite nanoparticles, and single-atom nanozymes, have exhibited remarkable peroxidase-like activity [5,6]. Prussian Blue nanoparticles synthesized through the reduction of a $FeCl_3$ and $K_3[Fe(CN)_6]$ mixture with hydrogen peroxide have demonstrated superior activity per catalytic unit compared to peroxidase [7]. This impressive catalytic activity, combined with the inexpensive and straightforward synthesis procedure, positions Prussian Blue nanoparticles as attractive substitutes for peroxidase. The mechanism underlying the peroxidase-like activity of Prussian Blue differs from that of horseradish peroxidase and involves the reduction of Prussian Blue to Prussian White by a chromogenic substrate (e.g., tetramethylbenzidine), followed by the oxidation of Prussian White back to Prussian Blue by hydrogen peroxide [8].

Controlling the size of Prussian Blue nanozymes is crucial for their application in various analytical techniques and *in vivo*. Larger nanoparticles contain more surface catalytic sites and can be covered with more recognition molecules [9,10]. On the other hand, smaller particles are better suited for applications requiring diffusion through porous membranes, such as lateral flow assays or paper microfluidics [11]. Selecting the optimal nanoparticle size is therefore an essential aspect of method optimization.

Given the significance of size control, there is a growing demand for methods that enable the synthesis of Prussian Blue nanoparticles with

tunable sizes. However, achieving small-sized nanoparticles poses a particular challenge [12]. One common approach to attaining smaller sizes involves ultrasonication of the reaction mixture [7,13]. In 2002, Liu et al. reported the preparation of Prussian Blue nanoparticles with a size of 50 nm by gradually adding 10 mM $FeCl_3$ to 10 mM $K_3[Fe(CN)_6]$ in the presence of a slight excess of hydrogen peroxide [14]. More recently, Karyakin's group developed a method for synthesizing Prussian Blue nanoparticles with sizes resembling proteins using reverse micelles [12].

The central idea of this study was to explore the feasibility of controlling the size of Prussian Blue nanoparticles through their synthesis in water-alcohol mixtures. The inspiration for this approach stemmed from the findings presented in the paper by Qin et al. [15]. In their work, the authors employed a solvothermal synthesis method to produce ultrasmall Prussian Blue nanoparticles (approximately 3.4 nm) using a single precursor, $K_3[Fe(CN)_6]$, in water-ethanol mixtures, with polyvinylpirrolidone serving as a capping agent. To date, no reports have emerged regarding the synthesis of Prussian Blue nanoparticles via the reductive method in water-alcohol mixtures.

A comprehensive literature search revealed several studies on the preparation of Prussian Blue nanoparticles [16–19], as well as Prussian Blue analogs [20–22], in various organic solvents such as formamide, ethanol, ethylene glycol, and methanol. In these studies, the exclusive use of solvothermal methods was observed. Interestingly, the incorporation of organic solvents, typically alcohols, generally resulted in significantly smaller particles compared to those prepared in water alone [16,18,20–22]. Another compelling aspect supporting the investigation of alcohols is their ability to influence crystal growth and reduce the rate of Ostwald ripening [23,24].

In this study, we embarked on the synthesis of Prussian Blue nanoparticles utilizing water/alcohol mixtures. Initially, we investigated the impact of volume fraction on the nanoparticle size for eight different alcohols, namely methanol, ethanol, propanol-1, isopropyl alcohol, tert-butanol, ethylene glycol, propylene glycol, and glycerol. Subsequently, we identified specific synthesis conditions (79.2% ethylene glycol and 52.8% methanol) that effectively reduced the nanoparticle size. We then proceeded to upscale the synthesis process by adjusting the precursor concentration and reaction volume accordingly. The upscaled method

yielded three batches of small-sized Prussian Blue nanoparticles, measuring 30-40 nm. These nanoparticles were subjected to comprehensive characterization, including evaluation of their physical-chemical properties such as size, surface area, elemental composition, and crystal structure. Furthermore, their peroxidase-like activity was compared with that of nanoparticles synthesized using the reducing method in pure water, as well as the traditional method involving the reaction between $FeCl_3$ and $K_4[Fe(CN)_6]$. Finally, we explored the practical application of the obtained small Prussian Blue nanoparticles as catalytic labels in an immunoassay targeting human SARS-CoV-2 antibodies.

2. Experimental section

2.1 Materials

Potassium hexacyanoferrate (III), Proclin-950, human IgG, hydrogen peroxide were from Sigma-Aldrich (USA). Iron (III) chloride hexahydrate, Tween-20, glutaraldehyde, ammonium hydroxide, citric acid, 3,3',5,5'-tetramethylbenzidine dihydrochloride, and glycerol (TMB) were from ITW (USA). Dialysis tubings (cellulose membrane; 10,000 MWCO) were from Thermo Scientific (USA). Tert-butanol, ethanol, and propanol-1 were from Reakhim (Russia). Methanol and ethylene glycol was from Vekton (Russia). Isopropyl alcohol was from Component-Reactiv (Russia). Propylene glycol was from Rushim (Russia). Bovine serum albumin was from Biosera (France). Mouse monoclonal IgG2a (against human prostate specific antigen), mouse monoclonal anti-human IgG antibodies, and recombinant spike protein of SARS-CoV-2 were obtained from HyTest (Finland). 96-well polystyrene plates (high binding) were from SPL Life Sciences (South Korea). Components of devices for vertical flow immunoassay: nitrocellulose membranes (CLW-040, 0.3 μm), absorbent pad AP-080 and plastic cases were from Advanced Microdevices Pvt. Ltd (India).

Blood serum samples were from our laboratory collection. Serum samples were obtained in 2022 in the framework of other projects dedicated to the study of post-vaccination immunity. Sera samples were stored at -20 °C. Antibodies against the spike protein of SARS-CoV-2 in these samples were detected by ELISA (Vektor-Best, Russia). Positive (>4000 BAU/mL) sera were pooled and used in the immunoassay of anti-spike IgG. This research was performed according to World Medical

Association's Declaration of Helsinki and Council of Europe Protocol to the Convention on Human Rights and Biomedicine and approved by the Ethics Committee of the Institute of Ecology and Genetics of Microorganisms, Ural Branch of the Russian Academy of Sciences (IRB00010009). Written informed consent was obtained from all the participants.

Instrumentation. Multiskan Sky UV-Vis Reader was from Thermo Scientific (USA). ZetaSizer NanoZS particle analyzer was from Malvern (UK). VCX-130 ultrasonic processor was from Sonics & Materials (USA).

2.2 Effect of alcohols

Synthesis of Prussian Blue nanoparticles was carried out in 16 mL glass vials in the water bath (Fig. S1). Bath temperature was +35 ℃. Reaction mixture was stirred (1000 rpm) using a 16 mm stir bar. Eight milliliters of water or water-alcohol mixture were added and kept for 10-15 minutes under stirring for temperature equilibration. Then, 91 μL of 300 mM $K_3[Fe(CN)_6]$, 91 μL of 300 mM $FeCl_3$, and 909 μL of 220 mM H_2O_2 have been successively added (in the experiment with 97% volume fraction of ethylene glycol H_2O_2 was diluted not with water but with ethylene glycol). We should note that the order of reagent addition affected the size of nanoparticles (Fig. S2) [25], therefore in all experiments it was as above. After an hour, the contents of the vial was transferred into dialysis tubing and dialyzed two times against distilled water and one time against deionized water. Total dialysis duration was about 48 hours. Resulting dilution of the sample was more than 200,000. At high alcohol concentrations samples intensively absorbed water and their volume increased from initial 9.09 mL to 10-15 mL. After dialysis, nanoparticle dispersions were transferred into thick-wall glass tubes. Before transfer, nanoparticles were carefully mixed using pipette, because in most of the samples aggregates settled on the bottom of dialysis tubing. Suspensions were sonicated on ice for 10 min (6 mm probe, amplification - 60%, actual power - 16-18 W) and stored at +4 ℃ in 15 mL plastic tubes. In some experiments, nanoparticles (usually 0.5-1 mL) were filtered through 0.22 and 0.1 μm MCE filters to remove larger particles. These samples were also kept at +4 ℃ in 1.5mL plastic tubes. Nanoparticle loss after filtration was assessed by spectrophotometer. 10 μL of nanoparticles before and after the filtration were added to the wells of 96-well flat-bottom

plate (3 wells per sample). Volume in all wells was adjusted to 200 µL with water. Absorbance at 700 was then measured.

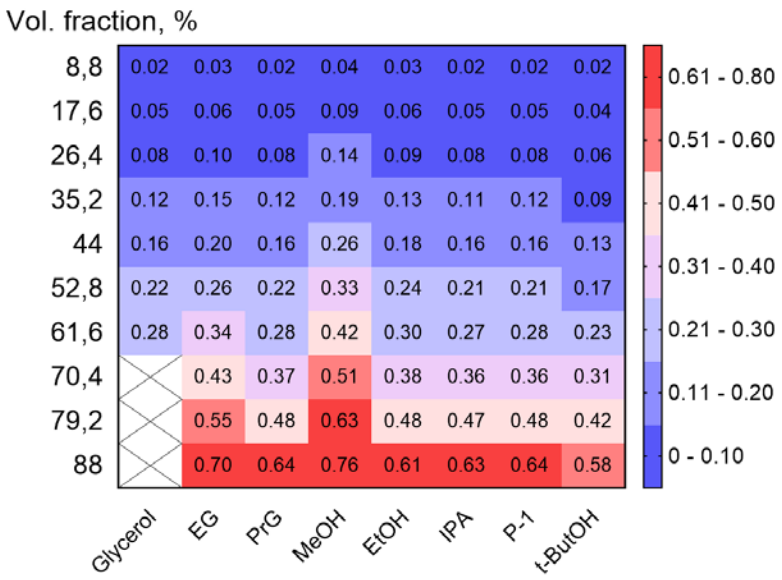

Fig. 1. Relationship between volume fraction and mole fraction for each water/alcohol mixture. Mole fraction values are given in cells. Note: For ethanol, the volume fractions were slightly smaller: 8.4%, 16.7%, 25.1%, 33.4%, 41.8%, 50.2%, 58.5%, 66.9%, 75.2%, and 83.6%.

Differential centrifugation. Nanoparticles synthesized in 70.4%, 79.2%, and 88% ethylene glycol and in 52.8% and 61.6% methanol were filtered through 0.22 µm MCE filter. Nanoparticles synthesized in water and 61.6% tert-butanol were not filtered. Then, all nanoparticles were diluted in water to 0.7-0.9 absorbance units at 700 nm. One milliliter of the resulting suspensions was centrifuged at 5000 g, 10000 g, or 15000g for 10 min. After that, absorbance at 700 nm was measured. Two technical replicates were prepared for each sample.

2.3 Synthesis of nanoparticles at a large scale

Synthesis of nanoparticles in 79.2% ethylene glycol with various concentrations of iron salts. In these experiments we used the same experimental setup. Ethylene glycol (8174 mg; 7364 µL) was added into a 16 mL glass vial and kept on the water bath for 30 min. Then, 409 µL of $K_3[Fe(CN)_6]$, 409 µL of $FeCl_3$, and 909 µL of H_2O_2 have been successively added. Resulting concentrations of iron salts were 1.5, 3, 6, 10, 20, and 30 mM. Molar concentrations of H_2O_2 in the final mixtures were 7-fold

higher (from 11 to 220 mM). The subsequent synthesis steps were the same.

Nanoparticles **EG-1**, **EG-2**, and **EG-3** were synthesized as follows. In a 250 mL glass beaker 144 mL of ethylene glycol, 3.28 mL of H_2O, 8.18 mL of 0.444 M $K_3[Fe(CN)_6]$, 8.18 mL of 0.444 M $FeCl_3$, and 18.18 mL of 1.46 M H_2O_2 have been successively added (Fig. S3). Addition of iron salts and peroxide and further synthesis were carried out on a magnetic stirrer at 1000 RPM. Duration of synthesis was 60 min. Temperature of the reaction medium was maintained at +35 °C using a temperature probe. After the synthesis was completed, powder of NaCl (1.16 g) was added and stirring speed was decreased to 300 RPM. Aggregation of nanoparticles was observed almost immediately. Suspension of nanoparticles was centrifuged at 4000 g for 5 min. Supernatants were discarded, sediment was resuspended in approximately 100 mL of water with the aid of brief sonication (6 mm probe, 60% amplification). Suspension was transferred into the dialysis tubing (cut off 10 kDa) and dialyzed for 5 days 4 times against 2 L of distilled water and 1 time against 2 L of deionized water. Dialyzed nanoparticles (approximately 120-130 mL) were divided into two equal parts. Each part was added into an 80 mL glass thick-walled round-bottom tube and sonicated on ice for 40 min (6 mm probe, 60% amplification). Then sonicated nanoparticles were united and stored at +4 °C.

Nanoparticles **W-1**, **W-2**, and **W-3** were synthesized as follows. In a 2 L glass beaker 800 mL of H_2O, 9.09 mL of 0.3 M $K_3[Fe(CN)_6]$, 9.09 mL of 0.3 M $FeCl_3$, and 90.8 mL of 0.22 M H_2O_2 have been successively added. Addition of iron salts and peroxide and further synthesis were carried out under stirring at 600 RPM (overhead stirrer). Duration of synthesis was 60 min. Temperature of the reaction medium was maintained at +35 °C using a temperature probe. After the synthesis was completed, powder of NaCl (5.3 g) was added and stirring speed was decreased to 300 RPM. Aggregation of nanoparticles was observed almost immediately. Suspension of nanoparticles was centrifuged at 4000 g for 5 min by portions of 50 mL. Supernatants were discarded, sediment was resuspended in approximately 60 mL of water with the aid of brief sonication (6 mm probe, 60% amplification). Suspension was transferred into the dialysis tubing (cut off 10 kDa) and dialyzed for 5 days 4 times against 2 L of distilled water and 1 time against 2 L of deionized water.

Dialyzed nanoparticles (approximately 70 mL) were sonicated on ice for 60 min (6 mm probe, 60% amplification) in 80 mL glass thick-walled round-bottom tube. Then sonicated nanoparticles were stored at +4 °C.

Nanoparticles **T-1**, **T-2**, and **T-3** were synthesized as follows. To 200 mL of 50 mM $K_4[Fe(CN)_6]$ 200 mL of 50 mM $FeCl_3$ have been quickly added under stirring at 700 RPM (magnetic stirrer). Both solutions were pre-warmed to +55 °C before mixing. Reaction was carried out for 10 min. Temperature or the mixture was maintained at +55 °C. After the synthesis was completed, isopropyl alcohol was added and stirring speed was decreased to 300 RPM. Aggregation of nanoparticles was observed almost immediately. Suspension of nanoparticles was centrifuged at 4000 g for 5 min by portions of 50 mL. Supernatants were discarded, sediment was resuspended in approximately 160 mL of water with the aid of brief sonication (6 mm probe, 60% amplification). Suspension was transferred into the dialysis tubing (cut off 10 kDa) and dialyzed for 5 days 4 times against 2 L of distilled water and 1 time against 2 L of deionized water. Dialyzed nanoparticles (approximately 200 mL) were sonicated on ice for 10 min (6 mm probe, 60% amplification) in 250 mL glass beaker. Then sonicated nanoparticles were stored at +4 °C.

2.4. Characterization of nanoparticles

Measurement of nanoparticle concentration. Nanoparticle suspensions (1 mL) were added to porcelain crucibles and dried first at +95 °C to evaporate water and then at +140 °C to constant weight. Mentioned temperature was chosen because Prussian Blue and its analogs do not decompose at this temperature [26,27].

Powder X-ray diffraction (XRD) and nitrogen adsorption analysis. Suspension of nanoparticles added in a glass beaker and dried for 10-12 h (depending on volume) at +80 °C [28] to complete water evaporation and then for another 10 h at the same temperature. Specific surface area was measured by analyzer Sorbi-M (META, Russia). XRD patterns were obtained using Empyrean (Malvern, UK).

UV-vis spectroscopy. Nanoparticles were diluted to 40 μg/mL in water and then their absorbance spectra were recorded at wavelengths between 200-1000 nm. Three spectra were recorded for each batch of nanoparticles. Averaged spectra are presented.

Elemental analysis. Concentration of iron and potassium in aqueous suspensions of nanoparticles measured by flame-atomic absorption spectrometry (flame-AAS) (spectrometer iCE 3500, Thermo, USA).

SEM and TEM images were obtained using Merlin (Carl Zeiss, Germany), Quanta 650FEG (FEI, USA), Hitachi HT7700 Excellence (Hitachi, Japan), and JEM-200CX (JEOL, Japan).

Catalytic activity. Optimization of the substrate buffer. Buffer which does not induce nanoparticle aggregation under short term exposure was determined. Three buffers were tested: 100 mM Na-acetate buffer, pH 4 with 0.1 mM Na_2-EDTA; 10 mM Na-acetate buffer, pH 4 with 0.1 mM Na_2-EDTA; 1 mM Na-acetate buffer, pH 4 with 0.01 mM Na_2-EDTA. Prussian Blue nanoparticles (batches **EG-3**, **W-3**, and **T-3**) were suspended in these buffers (40 μg/mL) and incubated for 10 min at room temperature. Size of nanoparticles was then measured by the DLS method (3 technical replicates for each condition). Suspensions of nanoparticles in water (40 μg/mL) were used for comparison. Only 1 mM buffer provided desirable stability of nanoparticles.

Demonstration of peroxidase- and oxidase-like activity. One milliliter of the substrate solution (1 mM Na-acetate buffer, pH 4; 0.01 mM Na_2-EDTA; 10% DMSO; 1 mg/mL TMB; with or without 0.03% H_2O_2) was added to 2.5 μL of 40 μg/mL Prussian Blue nanoparticle suspension. Absorbance at 562 nm was then measured for 5 min with 10 s intervals. Measurement was performed in 2 mL plastic cuvettes (1 cm pathlength) at room temperature (+28 ℃). Absorbance of the substrate buffer containing H_2O_2 was recorded under the same conditions.

Specific activity. Measurements were performed according to the recommendations [29,30] at room temperature (+27 ℃). Substrate solution (180 μL; 1 mM Na-acetate buffer, pH 4; 0.01 mM Na_2-EDTA; 10% DMSO; 1 mg/mL TMB; with or without 0.3% H_2O_2) was added to flat-bottom 96-well plates. 20 μL of aqueous nanoparticle suspensions was then added and quickly mixed with pipette tips. Absorbance at 652 nm was measured for 5 min with 6 s intervals. Resulting nanoparticle concentration was 100, 50, 25, 12.5, and 6.25 ng/mL. In control wells water without nanoparticles was added. Three technical replicates were made for each concentration. Concentration of product was determined from the equation:

$$c = \frac{A}{\varepsilon \times l}$$

where *c* is molar concentration, *A* is absorbance at 652 nm, ε is molar extinction coefficient (39000 $M^{-1} \times cm^{-1}$), l is pathlength (0.617 cm; measured as described in Supplementary Information). The absorbance of the control wells was subtracted in advance. The initial rate was determined by performing a linear regression of the product concentration against time, specifically focusing on the first 30 seconds of the reaction (Fig. S4). The specific activity was calculated as the slope of the initial rate versus nanoparticle weight regression line.

2.5. Conjugation of Prussian Blue nanoparticles with antibodies

Prussian Blue nanoparticles (**EG-1** or **W-2**) were dropwise added under vortexing to an aqueous BSA solution. Resulting concentrations of Prussian Blue and BSA were 2 mg/mL and 20 mg/mL, respectively. The mixture was sonicated for 10 min (3 mm probe, 80% amplification), and incubated at +37 ℃ on a rotator (10 rpm) for 60 min. Dispersion (4 mL) was dropwise added under vortexing to an equal volume of 25% glutaraldehyde, pH 7 (adjusted with 1 M NaOH) and incubated for 30 min at +37 ℃ on a rotator (10 rpm). Supernatant (8 mL) was applied to Sepharose CL-6B column pre-equilibrated with water (160 mL; d=26 mm, bed height - 30 cm) and eluted with water (elution speed - 0.65 mL/min). Fractions enriched with nanoparticles were combined. Collected nanoparticles (12 mL) were transferred into dialysis tubing (2 mL/cm, 10 kDa MWCO), covered with PEG 30kDa layer, and concentrated to 2.2 mL. Upon concentration formation of non-destroyable aggregates was observed. Dispersion of concentrated nanoparticles at 10000 g for 10 min (**W-2** nanoparticles were centrifuged at 1000 g for 10 min). Supernatant (1.8 mL, 2.33 mg/mL) was mixed with 200 µL of 0.1 M HEPES-HCl buffer, pH 7 and 74 µL of mouse anti-human MAbs (5.6 mg/mL) and vortexed. Conjugation proceeded at room temperature overnight on a rotator (10 rpm). BSA (20%) was added to 1% and incubation continued for one more hour. The mixture was centrifuged at 10000 g for 10 min (**W-2** nanoparticles were centrifuged at 1000 g for 10 min). Supernatant (2.2 mL) was sonicated applied to Sepharose CL-6B column pre-equilibrated with water (40 mL; d=16 mm, bed height - 20 cm), and eluted with water (elution speed - 0.25 mL/min). Fractions enriched with nanoparticles were

combined. Concentration of nanoparticles was monitored by measuring absorbance at 700 nm. Sample obtained after the cross-linking was used as a reference in absorbance measurements. Resulting nanoparticles were designated as EG-1/MAb and W-2/MAb.

2.6. Vertical flow immunoassay (VFI)

The nitrocellulose membrane was coated with spike protein (0.5 mg/mL, 2 µL) and human IgG (0.5 mg/mL, 2 µL) in a coating buffer. Then, the membranes were dried (30 min at room temperature and 90 min at +37 °C) and washed with 30 mL of washing solution for 5 minutes, three times. Next, the membrane was incubated with 35 mL of blocking solution (60 min, +37 °C) and washed. The membrane was dried, cut into small pieces (15×15 mm), and placed over 10 stacks of absorbent pads supported on a solid plastic case. Furthermore, the device was capped with a lid that had a hole for sample addition.

To carry out the VFI, all reagents were dropped onto the membrane through the hole sequentially. First, 150 µL of washing buffer was added until fully absorbed. Then, 100 µL of blood serum diluted tenfold with a blocking solution was added. After 1 minute of incubation and a second wash, 80 µL of EG-1/MAb or W-2/MAb in the blocking buffer at a concentration of 0.475 mg/mL was added. After 1 minute, the membrane was washed with 200 µL of washing solution. Subsequently, TMB substrate was added for signal enhancement. After 5 minutes, the assay results were visually evaluated and photographed.

The following buffers and solutions were used:

1. 0.01 M Phosphate-buffered saline (PBS): 0.137 mol/L NaCl + 0.0027 mol/L KCl, pH 7.4 (Ecoservice, Russia) + 0.53% ProClin950.
2. Coating buffer: PBS;
3. Washing solution: PBS + 0.1 % Tween-20;
4. Blocking solution: PBS + 0.2 % Tween-20;
5. TMB substrate: 9 mL of 0.1 M citrate/1 M NH_4OH buffer, pH 4 + 1 mL of 1 mg/mL TMB in DMSO + 85 µL of 35.3% H_2O_2.

3. Results and discussion

3.1. Effect of alcohols on the size of Prussian Blue nanoparticles

To investigate the impact of alcohols on the size of Prussian Blue nanoparticles, a series of experiments were conducted. The nanoparticles

were synthesized through the reduction of $K_3Fe[(CN)_6]/FeCl_3$ dissolved in water-alcohol mixtures with the addition of H_2O_2. As a starting point, three control batches of nanoparticles were prepared using pure water (Fig. S5). The hydrodynamic diameters (Dh) of these nanoparticles were found to be consistently similar, measuring 114, 115, and 118 nm. This observation indicates the reliable reproducibility of the synthesis procedure and highlights its suitability for studying the effect of solvents on nanoparticle size.

The alcohols tested in this study included methanol, ethanol, propanol-1, isopropyl alcohol, tert-butanol, ethylene glycol, propylene glycol, and glycerol. The volume fractions of these alcohols ranged from 8.8% to 79.2%, with higher concentrations also explored in some cases. The following paragraphs will discuss the results in terms of solvent effects on nanoparticle size, categorized into three groups: no effect, decrease, and increase. Plausible explanations for the observed patterns will be presented and discussed in section 3.5.

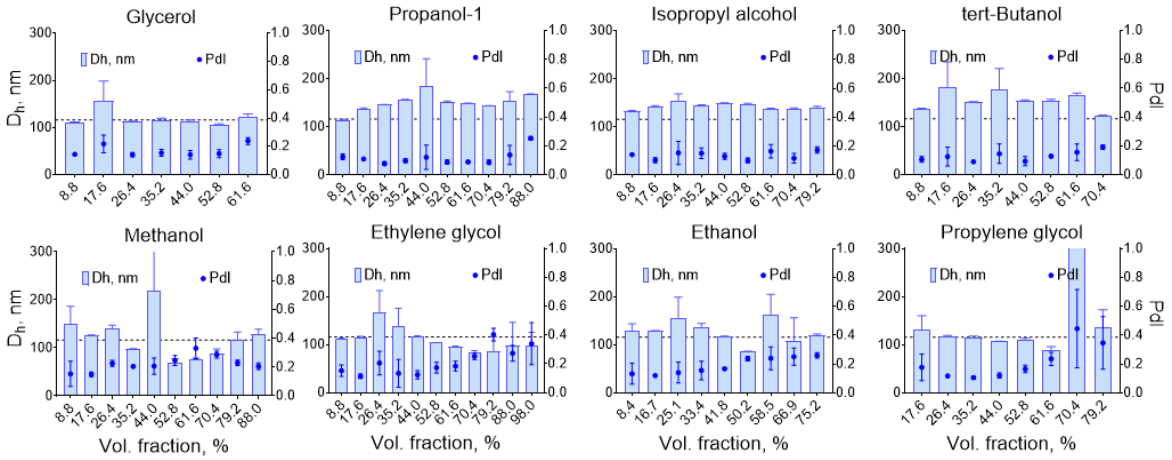

Fig. 2. Hydrodynamic diameters and polydispersity of Prussian Blue nanoparticles synthesized in different water/alcohol mixtures. The dashed line depicts the mean diameter of nanoparticles synthesized in pure water. n=3, mean±SD

Among all the alcohols tested, only glycerol had no discernible impact on the diameter of the Prussian Blue nanoparticles, regardless of its volume fraction (Fig. 2). However, when the volume fraction of glycerol exceeded 61.6%, the solvent became excessively viscous, hindering proper mixing of the reagents and impeding the formation of nanoparticles. Although no direct relationship between the concentration of glycerol and nanoparticle diameter was observed, this finding is

significant as it suggests that the viscosity of the solvent does not play a decisive role in the formation of Prussian Blue nanoparticles. It is worth noting that glycerol can function as both a reductant [31] and a regulator of nanoparticle size [32,33]. Thus, it is possible that the influence of viscosity was partially masked by the inherent effects of glycerol itself.

When it comes to methanol, ethanol, ethylene glycol, and propylene glycol, using these alcohols at volume fractions above 40-50% resulted in a decrease in the size of Prussian Blue nanoparticles compared to the control samples (Fig. 2 and Fig. S5). It is worth noting that the nanoparticle suspensions prepared under these conditions contained a certain percentage of larger nanoparticles or aggregates, as indicated by the increased polydispersity and variations in the dynamic light scattering (DLS) results between technical replicates (Fig. 2). However, by employing filtration to remove the aggregates, suspensions of small nanoparticles ranging from 50-90 nm with acceptable polydispersity (PdI of 0.2-0.3) could be obtained (Fig. 3A,B). For nanoparticles synthesized in methanol and ethylene glycol, the losses after filtration did not exceed 12-13% (Fig. 3A), indicating that the percentage of aggregates was not significant. Among the four alcohols mentioned, methanol and ethylene glycol proved to be the most suitable for obtaining small-sized Prussian Blue nanoparticles. Ethanol, on the other hand, resulted in only a slight reduction in Dh (20-30 nm below the control). While synthesis in propylene glycol yielded nanoparticles with a size of 54 nm, their overall yield was considerably lower compared to methanol or ethylene glycol (based on visual assessment of the color of the nanoparticle suspensions). Consequently, for further experiments, water/methanol (52.8 vol.%) and water/ethylene glycol (79.2 vol.%) mixtures were selected to obtain Prussian Blue nanoparticles with smaller sizes.

Mixtures of water with isopropyl alcohol, propanol-1, and tert-butanol resulted in the production of larger nanoparticles compared to water alone. However, there was no clear correlation between the hydrodynamic diameter and the concentration of alcohol. Typically, nanoparticles ranging from 130-170 nm were obtained at volume fractions above 17.6%.

At higher concentrations of certain alcohols, namely methanol (79.2%), ethanol (61.6%), propanol-1 (79.2%), isopropyl alcohol (79.2%), and tert-butanol (61.6%), cloudiness and the formation of aggregates

were observed in the reaction mixture even before the addition of H_2O_2. In cases where severe aggregation occurred, the samples were not further processed.

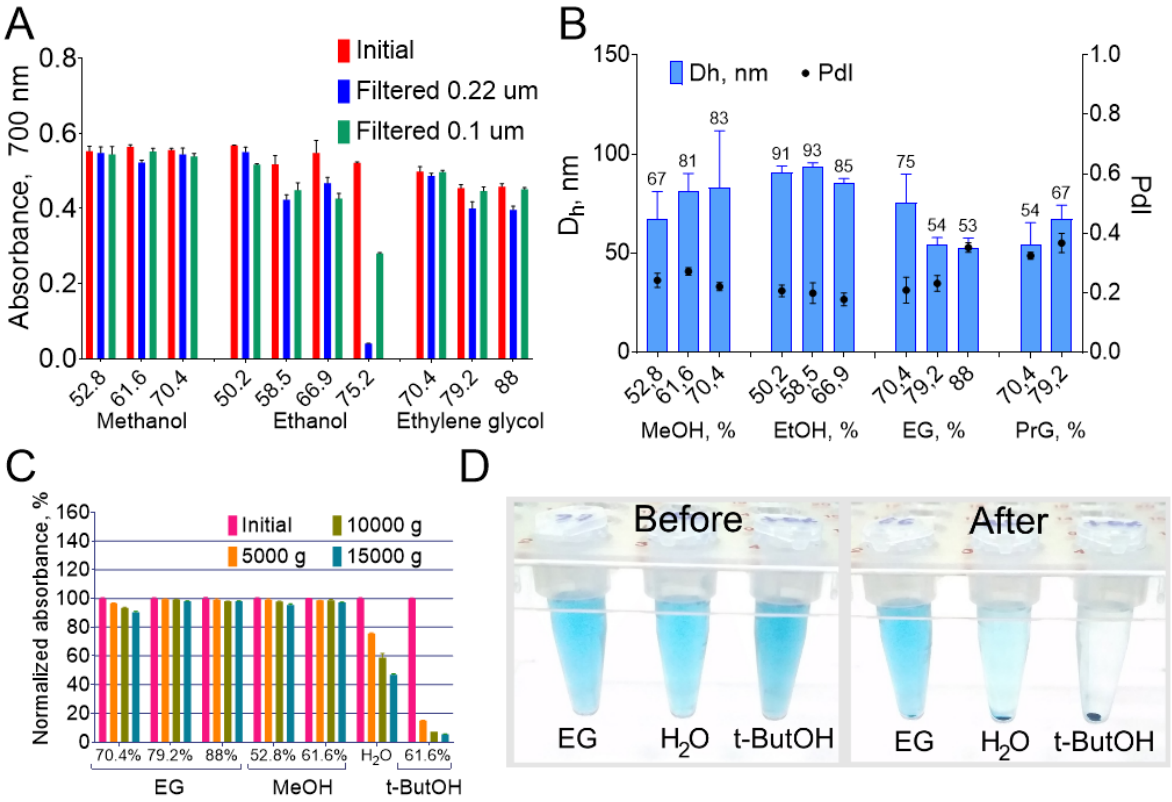

Fig. 3. (A) Loss of nanoparticles upon filtration. n=3, mean±SD. (B) Size and polydispersity of nanoparticles after filtration. n=3, mean±SD. (C, D) Study of nanoparticle size by differential centrifugation. (C) Percentage of the initial absorbance of supernatants. n=1. (D) Prussian Blue nanoparticles synthesized in different solvents (1 - 79.2% ethylene glycol, 2 - pure water, 3 - 61.6% tert-butanol) before (A) and after (B) centrifugation at 15,000 g.

In the described experiments, nanoparticle size was measured using dynamic light scattering (DLS). To further corroborate our findings, we also employed scanning electron microscopy (SEM) and conducted differential centrifugation. SEM analysis revealed that Prussian Blue nanoparticles exhibited spherical or quasi-spherical shapes, although irregular-shaped particles and aggregates were also observed in all samples (Fig. 4). It is worth noting that microscopic characterization of Prussian Blue nanoparticles prepared through the reductive route may not provide highly informative results, as distinguishing between individual nanoparticles can be challenging. However, a clear distinction was

observed between nanoparticles prepared in 79.2% ethylene glycol (Dh=54 nm) and those prepared in 61.6% tert-butanol (Dh=164 nm) (Fig. 4E,F).

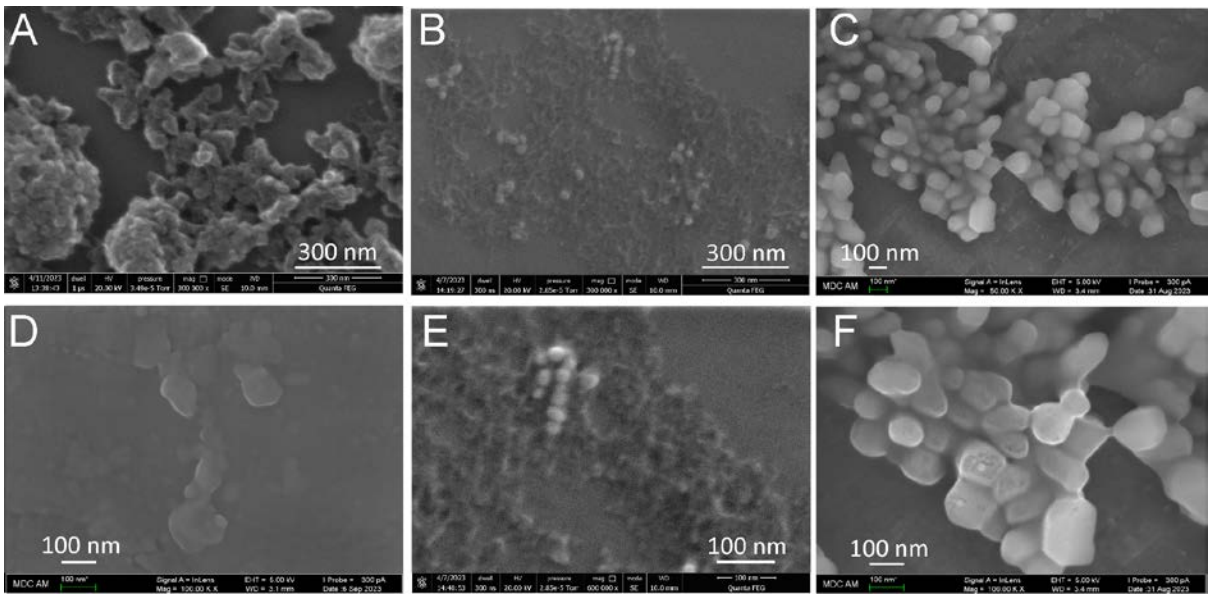

Fig. 4. SEM images of Prussian Blue nanoparticles synthesized in water (A, D), 79.2% ethylene glycol (B, E), and 61.6% tert-butanol (C, F).

Centrifugation of the nanoparticles at various acceleration levels confirmed the results obtained from DLS measurements (Fig. 3C, D). The extent of sedimentation of the nanoparticles was directly proportional to their size. Negligible sedimentation was observed for the smallest nanoparticles (Dh=50-80 nm according to DLS) even at an acceleration of 15,000 g. Conversely, nanoparticles synthesized in 61.6% tert-butanol (164 nm) settled almost completely at an acceleration of 5,000 g.

Thus, the initial part of our work demonstrates that synthesis at high volume fractions of ethylene glycol, propylene glycol, and methanol leads to the production of Prussian Blue nanoparticles that are more than two-fold smaller than those synthesized in water. However, there are several challenges that need to be addressed. The first issue pertains to the need for increasing the concentration of precursors and reaction volume to obtain a larger quantity of nanoparticles (scale-up). The second issue involves finding an alternative to the filtration procedure used to remove a small fraction of larger particles. While filtration is suitable for small volumes and diluted nanoparticle suspensions, it becomes ineffective when scaling up the reaction volume (20-fold) and increasing the precursor concentration (6-10-fold). One potential solution is to extend the

duration of the ultrasonication treatment. Therefore, the following section of the manuscript describes the results of our scale-up study.

3.2. Scale-up of nanoparticle synthesis

In the subsequent series of experiments, we investigated how increasing the reaction volume and iron salt concentration would impact the size of Prussian Blue nanoparticles synthesized in water/ethylene glycol and water/methanol mixtures. This information is crucial for the development of a synthesis scaling-up strategy.

To begin, we synthesized Prussian Blue nanoparticles in 79.2% ethylene glycol using ferric salts at concentrations ranging from 1.5 to 30 mM. The reaction volume remained consistent at 9 mL, as in the previous experiments. Previous studies have shown that the reductive synthesis in pure water leads to the production of larger Prussian Blue nanoparticles as the concentration of precursors increases [34]. We validated these findings by preparing Prussian Blue nanoparticles in water using $FeCl_3/K_3[Fe(CN)_6]$ at 20 and 30 mM. The resulting nanoparticles were approximately 1.5 times larger than those synthesized in the same 9 mL volume with 3 mM $FeCl_3/K_3[Fe(CN)_6]$ (Fig. 5).

In contrast, the presence of ethylene glycol effectively restricts nanoparticle growth, and even at a precursor concentration of 30 mM, the hydrodynamic diameter (Dh) remained at 54 nm (Fig. 5). To verify the reproducibility of our results, we repeated the synthesis of nanoparticles using 20 and 30 mM ferric salt solutions. At 30 mM of $FeCl_3/K_3[Fe(CN)_6]$, the Dh of the nanoparticles remained almost unchanged (53 nm), while at 20 mM, the Dh increased slightly to 60 nm.

When the synthesis was conducted in 52.8% methanol, we observed high turbidity in the reaction mixture after the addition of $K_3[Fe(CN)_6]$. This turbidity was likely caused by the limited solubility of the salt at such a high concentration of methanol. Surprisingly, the resulting nanoparticles exhibited nearly identical size (Dh=49 nm) and polydispersity compared to those prepared in ethylene glycol. It is important to note that in these experiments, larger nanoparticles were removed by filtration, as done previously. Overall, both the addition of ethylene glycol and methanol to the reaction mixture contribute to a reduction in the diameter of Prussian Blue nanoparticles. However, for subsequent experiments, we opted to utilize ethylene glycol to obtain

small Prussian Blue nanoparticles and avoid potential issues with the poor solubility of nanoparticle precursors.

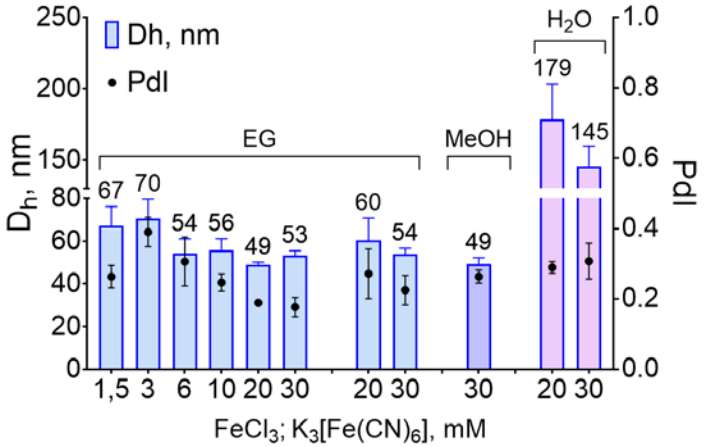

Fig. 5. Dependence of nanoparticle size on the initial concentration of iron salts. Nanoparticles were synthesized in 79.2% ethylene glycol (EG), 52.8% methanol (MeOH), and water. Two independent syntheses were performed in 79.2% ethylene glycol for 20 and 30 mM $FeCl_3$/$K_3[Fe(CN)_6]$. n=3, mean±SD.

Our next objective was to produce small Prussian Blue nanoparticles in a water-ethylene glycol mixture with a larger reaction volume. The concentration of iron salts was maintained at 20 mM, while the volume of the reaction medium was increased 20-fold to 180 mL. Due to the substantial quantity of nanoparticles generated, it was impractical to remove aggregates using a syringe filter. Therefore, we explored the possibility of achieving a sufficient degree of aggregate removal through extended sonication. Remarkably, increasing the sonication time from 10 to 40 minutes resulted in an almost 1.5-fold decrease in the hydrodynamic diameter of the nanoparticles, while the polydispersity remained unaffected (Fig. S6A).

Employing this approach, we synthesized three batches (**EG-1**, **EG-2**, and **EG-3**) of Prussian Blue nanoparticles with hydrodynamic diameters of 39 nm, 36 nm, and 32 nm, respectively. Each separate synthesis yielded approximately 700-800 mg of nanoparticles from the 180 mL reaction medium. For the sake of comparison, we also synthesized Prussian Blue nanoparticles using the reductive method in pure water (batches **W-1**, **W-2**, and **W-3**) and by the traditional method involving the reaction between $FeCl_3$ and $K_4[Fe(CN)_6]$ (batches **T-1**, **T-2**, and **T-3**). These nanoparticles were also subjected to extensive sonication until their

sizes reached values comparable to those obtained in the small-scale experiments (Fig. S6B).

The nanoparticles were characterized using various techniques, including dynamic light scattering (DLS), scanning electron microscopy (SEM), transmission electron microscopy (TEM), X-ray diffraction (XRD), UV-Vis spectroscopy, flame atomic absorption spectroscopy (AAS), nitrogen adsorption (BET), and differential centrifugation.

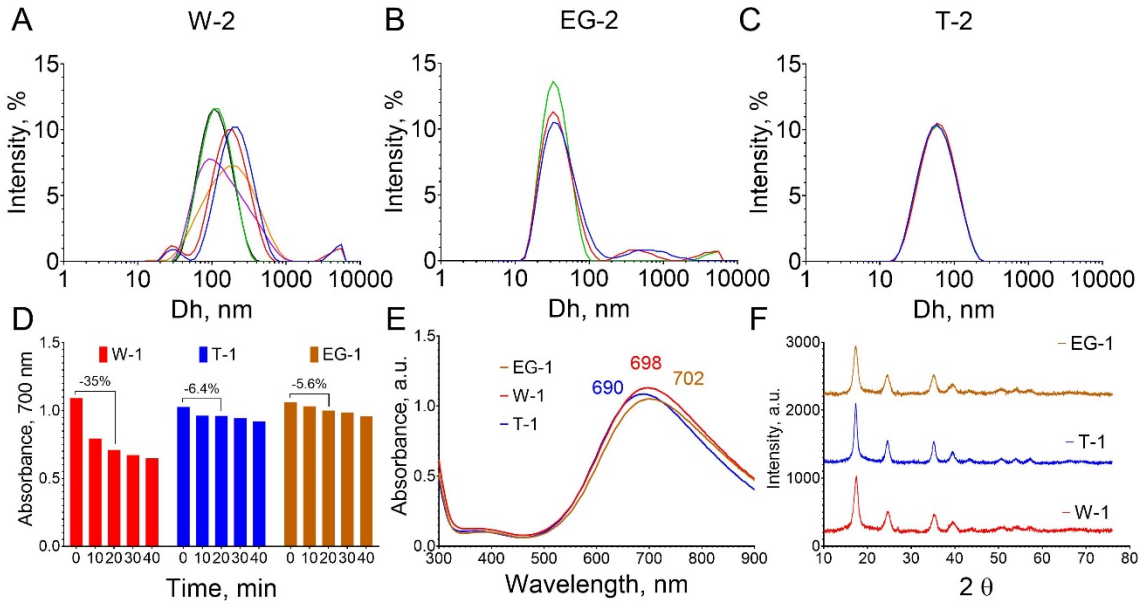

Fig. 6. Properties of Prussian Blue nanoparticles: (A-C) DLS intensity-weighted size distributions (size distributions of technical replicates are shown), (D) sedimentation rate, (E) UV-Vis spectra, and (F) XRD patterns. n=6 (A), n=3 (B,C), n=1 (D), mean±SD.

X-ray diffraction analysis of all the samples examined exhibited the characteristic pattern of Prussian Blue (JCPDS no. 73-0687). The samples were found to be crystalline, with a crystallite size of approximately 8 nm (Fig. 6F and Fig. S7). The UV-Vis absorption spectra also displayed typical features of Prussian Blue, albeit with slight variations among the different types of nanoparticles (Fig. 6E and Fig. S8). Nanoparticles synthesized using the traditional approach (**T**) exhibited a blue-shifted absorbance peak (690.3±0.6 nm) in comparison to those synthesized in ethylene glycol (**EG**) (698.7±3.1 nm) and water (**W**) (697.0±1.0 nm) through the reductive approach. This blue shift is likely attributed to the higher potassium content in the traditionally synthesized nanoparticles (see **Table 1**) [35].

Hydrodynamic diameters of the nanoparticles were measured using DLS, yielding values of 32-39 nm for **EG**, 102-126 nm for **W**, and 49-57 nm for **T**. It is important to note that DLS measurements often tend to overestimate the size of nanoparticles [28]. Therefore, we also analyzed the nanoparticles using SEM and TEM to obtain complementary information (Fig. 7). However, it is worth mentioning that determining the precise size of Prussian Blue nanoparticles through microscopy is a challenging task, as the boundaries of the nanoparticles are not easily distinguishable. This limitation is consistent with findings reported by other researchers (e.g., Fig. 1 in [36] or Fig. S3 in [37]). Consequently, we will primarily focus on providing a qualitative assessment of the SEM and TEM images and interpret them in conjunction with the results obtained from DLS and differential centrifugation.

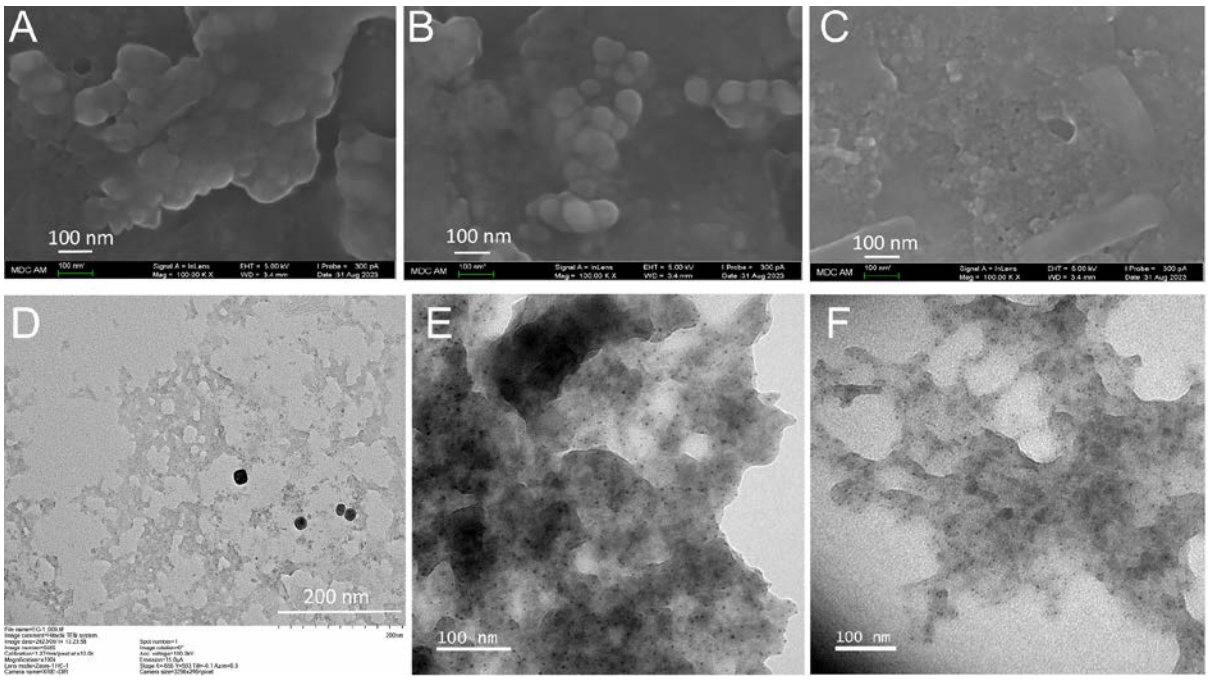

Fig. 7. SEM images of (A) EG-1, (B) W-1, and (C) T-1. TEM images of (D) EG-1, (E) W-1, and (F) T-1 nanoparticles.

The results obtained from DLS revealed a significant difference in size between the **T** and **EG** nanoparticles compared to the **W** nanoparticles, with a 2-3-fold difference. Notably, the reproducibility of DLS measurements between technical replicates for the **W** nanoparticles was poor (Fig. 6A), indicating the presence of large nanoparticles. However, SEM analysis did not exhibit a substantial distinction between the **W** and **EG** samples, as both displayed spherical particles with a

diameter of approximately 100 nm (Fig. 7A,B). Conversely, the TEM images clearly showcased the difference between the **EG** and **W** nanoparticles, with the **EG** nanoparticles appearing much smaller (Fig. 7D,E). Interestingly, the TEM images of the **W** and **T** samples did not reveal distinguishable individual large nanoparticles (tens of nanometers), but rather appeared as a homogeneous mass (Fig. 7E,F). However, since other analytical methods did not detect such large particles, we conclude that what is observed is indeed a mass of nanoparticles and not microscale aggregates. Importantly, TEM analysis uncovered the presence of numerous very small nanoparticles (less than 10 nm), which can be observed as black dots in the images, within both the **W** and **T** samples. These nanoparticles were markedly different from the surrounding "nanoparticle mass." Therefore, based on the microscopy analysis and DLS results, we concluded that all the samples contained very small nanoparticles with sizes below 10 nm, as well as a fraction of larger nanoparticles. The size distribution and percentage of these larger nanoparticles primarily determined the hydrodynamic diameter measured by DLS, as this technique is more sensitive to larger nanoparticles. This hypothesis was further supported by differential centrifugation experiments (Fig. 6D). The nanoparticles were subjected to centrifugation at 20,000 g for 10-40 minutes, and the sedimentation rate was evaluated by measuring the absorbance of the supernatant at 700 nm. The supernatant of the **W-1** sample exhibited a 35% decrease in absorbance after 20 minutes, whereas only a 5-6% decrease was observed in the **T-1** and **EG-1** samples. Subsequent centrifugation cycles resulted in a gradual decline in the absorbance of the supernatant for all the samples. These findings suggest that the **W** contained a significant portion of larger nanoparticles (approximately 30%), which were absent or negligible in the **T** and **EG**. Therefore, the addition of ethylene glycol appears to prevent the formation of larger nanoparticles/aggregates rather than simply reducing the size of the nanoparticles.

Table 1. Properties of Prussian Blue nanoparticles

	Dh, nm (n=3, mean±SD)	**PdI (n=3, mean±SD)**	**Abs. peak, nm**	**Fe, weight%**	**K, weight%**	**Specific surface, $m^2 \times g^{-1}$**
EG-1	39.4±4.4	0.254±0.027	702	23.67	0.54	9.9

EG-2	36.2±2.8	0.249±0.047	696	24.06	1.63	15.7
EG-3	32.1±3.1	0.187±0.055	698	24.28	1.65	11.2
W-1	102.8±7.2	0.226±0.044	698	25.31	0.51	23.1
W-2	128.2±30.6	0.285±0.081	697	23.77	0.48	14.4
W-3	126.9±28.2	0.190±0.069	696	24.54	0.47	23.8
T-1	49.2±0.8	0.208±0.027	690	24.16	6.33	156
T-2	53.1±1.1	0.206±0.008	690	23.16	6.16	178
T-3	57.5±2.2	0.207±0.036	691	23.11	6.46	182

3.3. Catalytic activity of Prussian Blue nanoparticles

All the different types of Prussian Blue nanoparticles synthesized in this study exhibited peroxidase-like activity, as demonstrated by their ability to oxidize TMB in the presence of H_2O_2 (Fig. 8A-C). However, no oxidation of TMB was observed in solutions without H_2O_2, indicating that Prussian Blue nanoparticles do not possess oxidase-like activity in TMB-containing substrates. This selectivity has been previously reported and is attributed to differences in redox potentials between TMB and Prussian Blue [8].

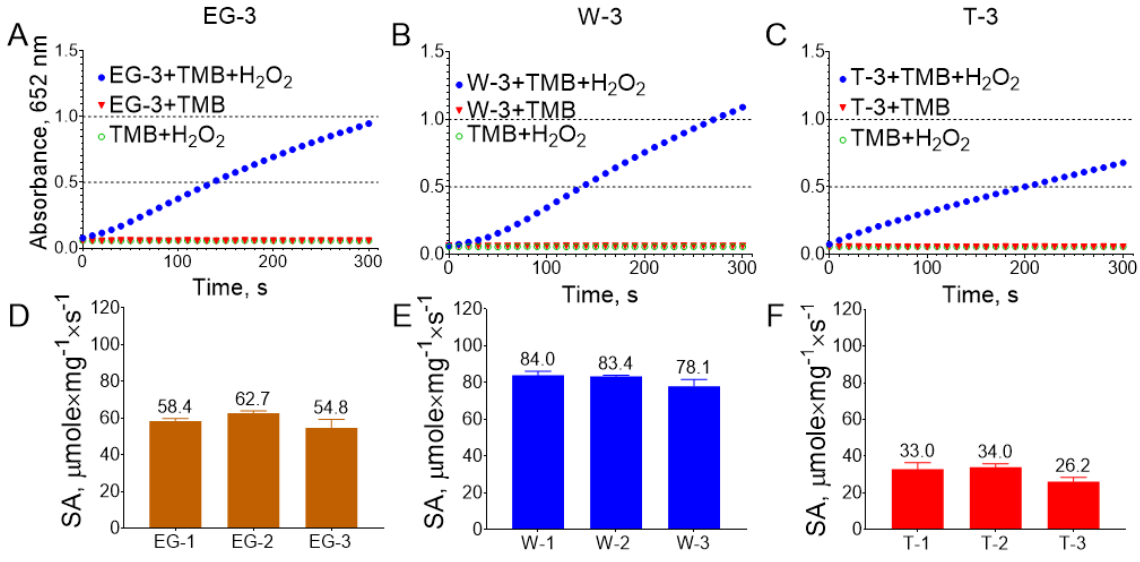

Fig. 8. Peroxidase- and oxidase-like activity, n=1 (A-C) and specific activity, n=3, mean±SD (D-F) of Prussian Blue nanoparticles.

The comparison of the catalytic properties of the Prussian Blue nanoparticles was conducted by measuring their specific activity, which

refers to the rate of substrate conversion per unit weight (Fig. 8D-F). As expected, the specific activity of the nanoparticles synthesized through the reductive approach (**W** and **EG**) was approximately 3-fold and 2-fold higher, respectively, compared to that of **T.** Therefore, the synthesis of Prussian Blue nanoparticles in an ethylene glycol-water mixture yields small nanoparticles with high catalytic activity.

The reasons behind the higher catalytic activity of the Prussian Blue nanoparticles synthesized through the reductive method remain unknown. It can be observed from the results of DLS and electron microscopy that there is no direct relationship between the size of the nanoparticles and their activity. To investigate whether **W** and **EG** have a larger specific surface area, we employed the nitrogen adsorption method. Interestingly, the specific surface area of **T** was nearly one order of magnitude larger (156-182 m^2/g) than that of **W** (14.4-23.8 m^2/g) and **EG** (9.9-15.7 m^2/g). However, no distinct correlation was found between the specific surface area and the activity. This finding aligns with the observations made by Komkova et al. [7], who demonstrated that the peroxidase-like activity of Prussian Blue nanoparticles is proportional to the third power of their diameter, suggesting that not only the surface iron atoms but also the inner parts of the nanoparticles participate in the catalytic process.

Another factor contributing to the peroxidase-like activity of the nanoparticles is their crystallinity, as amorphous nanoparticles tend to exhibit higher activity [38,39]. However, as mentioned earlier, the X-ray diffraction patterns obtained for **W**, **EG**, and **T** nanoparticles were almost identical. The only notable difference among the three types of nanoparticles was the potassium content. The interstitial sites of the Prussian Blue lattice can accommodate various alkaline cations, such as K^+, Na^+, NH^{4+}, etc. In this study, we synthesized Prussian Blue using $K_3[Fe(CN)_6]$ or $K_4[Fe(CN)_6]$ as precursors, and thus the potassium content was measured in all the samples using AAS. Generally, the peroxidase-like activity showed an inverse relationship with the potassium percentage. However, the mechanism underlying the effect of potassium is yet to be studied. The higher catalytic activity of **W** compared to **EG** can also be attributed to the presence of adsorbed ethylene glycol molecules on the surface of **EG** nanoparticles, which may screen the surface catalytic sites [40].

3.4. Application of small-sized Prussian Blue nanoparticles

As mentioned in the Introduction, controlling the size of Prussian Blue nanoparticles is crucial for their application as catalytic labels in immunoassays. Rapid paper-based tests, such as lateral flow and vertical flow immunoassays (VFI), require the easy migration of nanosized tags through the pores of the membrane. The presence of large nanoparticles can cause membrane clogging, resulting in high background signals and, consequently, reduced detection limits and false-positive results. In this section, we conducted a comparison of the background signals generated in a VFI using detection reagents prepared from **W-2** and **EG-1** nanoparticles.

The **EG-1** nanoparticles (39 nm) and **W-2** nanoparticles (128 nm) were coated with a layer of BSA and conjugated with monoclonal mouse anti-human antibodies (MAb). These modified nanoparticles were referred to as EG-1/MAb and W-2/MAb, respectively. The size distribution of the functionalized nanoparticles was similar to that of the parent nanoparticles, with a slight increase in the mean diameter (by 4-5 nm) due to the presence of the attached BSA and antibodies (Table S1). The specificity of the conjugates to human IgG was confirmed through ELISA (Fig. S9).

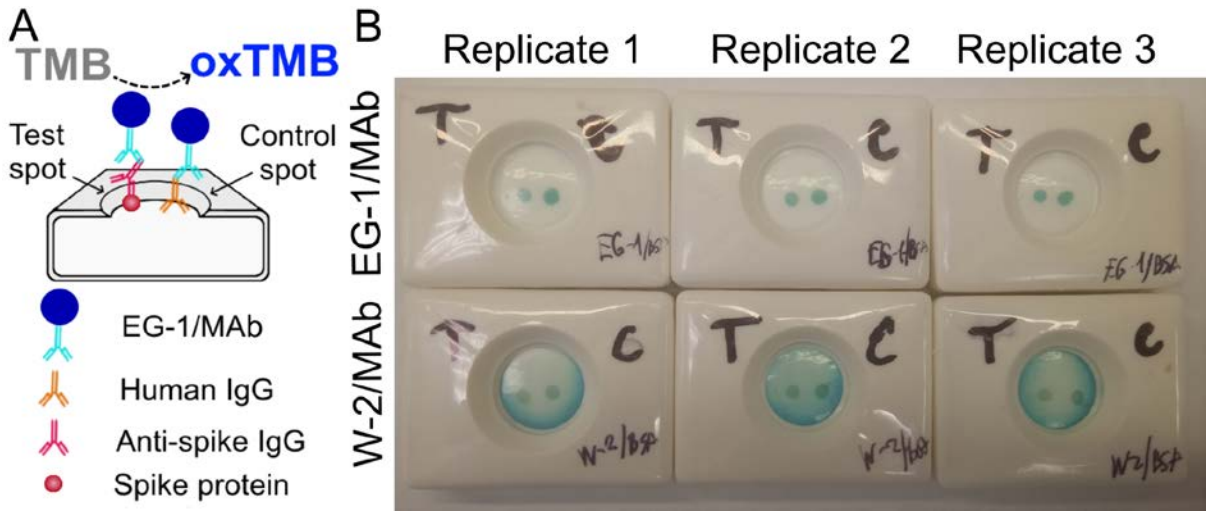

Fig. 9. Application of EG-1/MAb and W-2/MAb in VFI. (A) Scheme of the assay; (B) VFI of human anti-spike IgG in human blood serum. T - test spot; C - control spot.

The conjugates were employed as detection reagents in the vertical flow immunoassay (VFI) for human antibodies against the spike protein of

the coronavirus. The VFI membranes, with a pore size of 3 μm, were coated with the spike protein (test spot) and human IgG (control spot). Subsequently, serum from individuals vaccinated against SARS-CoV-2, Prussian Blue conjugates, and the TMB substrate were added sequentially (Fig. 9A). Both types of Prussian Blue conjugates were able to detect anti-spike antibodies. However, it was observed that EG-1/MAb generated a significantly lower background signal compared to W-2/MAb (Fig. 9B). This finding confirms that the synthesis of Prussian Blue nanoparticles in ethylene glycol effectively reduces their size, making them small enough for application in paper-based assays.

3.5. Possible mechanisms of alcohols effect

The size of nanoparticles prepared from molecular precursors is influenced by the balance between nucleation, the growth of nuclei, and their coalescence [41]. It is known from the literature that the formation of Prussian Blue nanoparticles also involves the assembly of smaller nanoparticles into larger ones, which can transform from loose assemblies to solid particles upon aging [42]. We acknowledge that the formation of Prussian Blue nanoparticles in water/alcohol mixtures is a complex process, and numerous factors contribute to the size and yield of the resulting nanoparticles. In this study, our aim was not to extensively investigate the mechanism of nanoparticle formation. However, we will discuss possible ways in which alcohols can affect the growth of nanoparticles.

Firstly, the viscosity of alcohol/water mixtures differs from that of water and depends on both the alcohol structure and its concentration. Increasing the volume fraction of alcohol leads to changes in viscosity. For certain alcohols, this relationship is direct (e.g., for ethylene glycol and glycerol [43,44]), while for others, it is more complex (e.g., for ethanol, methanol, and propanol-1 [45]). Previous studies have shown that the decrease in nanoparticle size at higher glycerol concentrations can be attributed to slower diffusion of precursors to pre-formed particles [24], thereby limiting their growth and resulting in a lower yield. However, in our study, we did not observe a distinct dependence of nanoparticle size on viscosity. As mentioned in the section 3.1, synthesis in the most viscous solvent, water/glycerol, had no effect on nanoparticle size. Water/isopropyl alcohol mixtures yielded large nanoparticles, while

synthesis in water/ethylene glycol with the same viscosity produced nanoparticles that were not different from the control samples.

Another potential mechanism is the reduction of Prussian Brown, which forms after the reaction between Fe^{3+} and $[Fe(CN)_6]^{3-}$, by alcohols themselves. Upon the addition of iron salts to the water/alcohol mixture, the solution became dark brown, indicating the formation of Prussian Brown ($Fe^{III}[Fe^{III}(CN)_6]$), which possesses the same cubic elemental unit as Prussian Blue [46]. Notably, the color of the solution was more intense at higher alcohol volume fractions. In the case of high volume fractions of ethylene glycol and propylene glycol (>70%), the solution quickly changed to a dark greenish-blue color, indicating the rapid formation of Prussian Blue. Although the time gap between the addition of iron salts and the main reductant, hydrogen peroxide, usually did not exceed 10 seconds, the reduction of Prussian Brown by alcohol molecules could potentially initiate the formation of multiple nuclei. These pre-formed nuclei and particles could influence the overall process. To investigate this, we assessed the ability of alcohols to reduce Prussian Brown to Prussian Blue by measuring the absorption spectrum between 500 and 900 nm one minute after the addition of $FeCl_3$ and $K_3[Fe(CN)_6]$ to the water/alcohol mixtures. Distinct broad peaks around 800 nm were observed for the highest volume fractions of methanol, ethylene glycol, and propylene glycol (Fig. S10). This peak represents a partial reduction of Prussian Brown to Prussian Green and Prussian Blue [2,47]. Visual observation of the samples after the experiment (Fig. S11-S14) confirmed the results of spectroscopy, as green and blue products were observed in samples containing glycerol, methanol, ethylene glycol, and propylene glycol, where the intensity of the color was proportional to the volume fraction of alcohol. Other alcohols did not cause such rapid reduction, although blue product formation was observed in all samples after several hours. Therefore, the ability of alcohols to decrease the size of Prussian Blue nanoparticles generally aligns with their reducing properties, except for ethanol.

Another factor that could potentially influence the size of the nanoparticles is the adsorption of alcohols on the surface of growing nanoparticles, which can impede their growth and limit Ostwald ripening [23]. As previously mentioned, the formation of polycrystalline Prussian Blue nanoparticles through the assembly of monocrystalline nanoparticles

is a common process. In our study, we indeed observed larger particles on TEM and SEM images beyond the crystallite size obtained from XRD analysis for all the samples. Hence, alcohols may hinder both the growth of primary nuclei and their subsequent coalescence. Specifically, ethylene glycol and propylene glycol can chelate the metal precursors of the nanoparticles and impede the coalescence of nuclei or small nanoparticles [48,49]. On the other hand, alcohols can facilitate the growth of nanoparticles by desolvating the precursors, making it easier for them to collide with previously formed crystals [50,51]. In our study, the effect of alcohols generally correlated with their dielectric constants (Table S2) and chaotropicity/cosmotropicity [52]. Consistent with the findings of Song et al. [51], more hydrophobic alcohols (such as t-butanol, isopropyl alcohol, and propanol-1) promoted the growth of nanoparticles, whereas more hydrophilic alcohols decreased the nanoparticle diameter.

Other factors, such as the solubility of precursors and the colloidal stability of Prussian Blue nanoparticles, could also contribute to the alteration of the resulting nanoparticle size. For instance, we observed the sedimentation of iron salts upon their addition to solutions with a high volume fraction of alcohols (e.g., 80% isopropyl alcohol, 70% t-butanol, 90% methanol, 90% propanol-1).

4. Conclusion

This work showcases the utilization of water/alcohol mixtures in the preparation of Prussian Blue nanoparticles with tunable sizes. Depending on the alcohol's structure and concentration, both larger and smaller nanoparticles can be achieved. The primary focus of this study was on the synthesis of small-sized nanoparticles. One important discovery is that the synthesis in water/ethylene glycol and water/methanol mixtures enables an increase in precursor concentration and reaction volume without affecting the mean diameter of the resulting nanoparticles. This finding holds immense significance in terms of the scalability of the presented technology, which is a major hurdle in implementing nanoparticles into practical applications. Notably, the proposed method for controlling nanoparticle size does not necessitate the addition of polymer stabilizers, thereby providing more options for the post-synthetic functionalization. Potentially, the synthesis in water/alcohol mixtures is not limited to Prussian Blue alone; it can be extended to Prussian Blue analogs and

other cyano-bridged coordination polymers. The potential applications of these materials span various fields, including energy storage, catalysis, electrochemistry, and theranostics [53].

CRediT authorship contribution statement

Pavel Khramtsov: Investigation, Writing – original draft. Maria Kropaneva: Investigation, Funding acquisition, Dmitry Kiselkov: Investigation, Artem Minin: Investigation, Larisa Chekanova: Investigation, Mikhail Rayev: Conceptualization, Supervision, Writing – original draft, Writing – review & editing.

Declaration of Competing Interest

The authors declare that they have no known competing financial interests or personal relationships that could have appeared to influence the work reported in this paper.

Data Availability

No data was used for the research described in the article.

Declaration of Generative AI and AI-assisted technologies in the writing process

During the preparation of this work, the authors used OpenAI's tool, ChatGPT 3.5, to check grammar and rephrase certain sentences. The initial text was written in English by human authors. After applying ChatGPT, the authors diligently reviewed and edited the content as necessary, taking full responsibility for the publication's content.

Acknowledgements

This research was funded by the Russian Science Foundation, grant number 22-75-00025

Transmission electron microscopy investigations were performed in the Collaborative Access Center of the M.N. Mikheev Institute of Metal Physics of the Ural Branch of the Russian Academy of Sciences.

The authors thank the Core Facility of the Perm Federal Research Center of the Ural Branch of the Russian Academy of Sciences.

References

[1] A. Ludi, Prussian blue, an inorganic evergreen, J. Chem. Educ. 58 (1981) 1013. https://doi.org/10.1021/ed058p1013.
[2] K. Itaya, I. Uchida, Nature of intervalence charge-transfer bands in Prussian blues, Inorg. Chem. 25 (1986) 389–392. https://doi.org/10.1021/ic00223a034.
[3] A. Kraft, Some considerations on the structure, composition, and properties of Prussian blue: a contribution to the current discussion, Ionics. 27 (2021) 2289–2305. https://doi.org/10.1007/s11581-021-04013-0.
[4] M.A. Komkova, A.A. Karyakin, Prussian blue: from advanced electrocatalyst to nanozymes defeating natural enzyme, Microchim. Acta. 189 (2022) 290. https://doi.org/10.1007/s00604-022-05363-w.
[5] Z. Chi, Q. Wang, J. Gu, Recent advances in colorimetric sensors based on nanozymes with peroxidase-like activity, Analyst. 148 (2023) 487–506. https://doi.org/10.1039/D2AN01850K.
[6] X. Wang, X.J. Gao, L. Qin, C. Wang, L. Song, Y.-N. Zhou, G. Zhu, W. Cao, S. Lin, L. Zhou, K. Wang, H. Zhang, Z. Jin, P. Wang, X. Gao, H. Wei, eg occupancy as an effective descriptor for the catalytic activity of perovskite oxide-based peroxidase mimics, Nat. Commun. 10 (2019) 704. https://doi.org/10.1038/s41467-019-08657-5.
[7] M.A. Komkova, E.E. Karyakina, A.A. Karyakin, Catalytically Synthesized Prussian Blue Nanoparticles Defeating Natural Enzyme Peroxidase, J. Am. Chem. Soc. 140 (2018) 11302–11307. https://doi.org/10.1021/jacs.8b05223.
[8] M.A. Komkova, O.A. Ibragimova, E.E. Karyakina, A.A. Karyakin, Catalytic Pathway of Nanozyme “Artificial Peroxidase” with 100-Fold Greater Bimolecular Rate Constants Compared to Those of the Enzyme, J. Phys. Chem. Lett. 12 (2021) 171–176. https://doi.org/10.1021/acs.jpclett.0c03014.
[9] M. Broto, M.M. Kaminski, C. Adrianus, N. Kim, R. Greensmith, S. Dissanayake-Perera, A.J. Schubert, X. Tan, H. Kim, A.S. Dighe, J.J. Collins, M.M. Stevens, Nanozyme-catalysed CRISPR assay for preamplification-free detection of non-coding RNAs, Nat. Nanotechnol. 17 (2022) 1120–1126. https://doi.org/10.1038/s41565-022-01179-0.
[10] L. Rivas, L. Hu, C. Parolo, A. Idili, A. Merkoçi, Rational Approach to Tailor Au–IrO2 Nanoflowers as Colorimetric Labels for Lateral Flow Assays, ACS Appl. Nano Mater. 6 (2023) 4151–4161. https://doi.org/10.1021/acsanm.2c04915.
[11] X. Chen, L. Ding, X. Huang, Y. Xiong, Tailoring noble metal nanoparticle designs to enable sensitive lateral flow immunoassay,

Theranostics. 12 (2022) 574–602. https://doi.org/10.7150/thno.67184.
[12] V.N. Nikitina, M.D. Zavolskova, A.A. Karyakin, Protein-sized nanozymes «artificial peroxidase» based on template catalytic synthesis of Prussian Blue, Bioelectrochemistry Amst. Neth. 149 (2023) 108275. https://doi.org/10.1016/j.bioelechem.2022.108275.
[13] P.A. Fiorito, V.R. Gonçales, E.A. Ponzio, S.I.C. de Torresi, Synthesis, characterization and immobilization of Prussian blue nanoparticles. A potential tool for biosensing devices, Chem Commun. (2005) 366–368. https://doi.org/10.1039/B412583E.
[14] S.-Q. Liu, J.-J. Xu, H.-Y. Chen, Electrochemical behavior of nanosized Prussian blue self-assembled on Au electrode surface, Electrochem. Commun. 4 (2002) 421–425. https://doi.org/10.1016/S1388-2481(02)00336-3.
[15] Z. Qin, B. Chen, Y. Mao, C. Shi, Y. Li, X. Huang, F. Yang, N. Gu, Achieving Ultrasmall Prussian Blue Nanoparticles as High-Performance Biomedical Agents with Multifunctions, ACS Appl. Mater. Interfaces. 12 (2020) 57382–57390. https://doi.org/10.1021/acsami.0c18357.
[16] D. Su, A. McDonagh, S.-Z. Qiao, G. Wang, High-Capacity Aqueous Potassium-Ion Batteries for Large-Scale Energy Storage, Adv. Mater. Deerfield Beach Fla. 29 (2017). https://doi.org/10.1002/adma.201604007.
[17] W. Geng, Z. Zhang, Z. Yang, H. Tang, G. He, Non-aqueous synthesis of high-quality Prussian blue analogues for Na-ion batteries, Chem Commun. 58 (2022) 4472–4475. https://doi.org/10.1039/D2CC00699E.
[18] S. Wang, M. Qin, M. Huang, X. Huang, Q. Li, Y. You, Organic Solvothermal Method Promoted Monoclinic Prussian Blue as a Superior Cathode for Na-Ion Batteries, ACS Appl. Energy Mater. 5 (2022) 6927–6935. https://doi.org/10.1021/acsaem.2c00536.
[19] J. Yang, Z. Huang, B. Yang, H. Lin, L. Qin, M. Nie, Q. Li, Green route to Prussian blue nanoparticles with high degradation efficiency of RhB under visible light, J. Mater. Sci. 56 (2021) 3268–3279. https://doi.org/10.1007/s10853-020-05406-8.
[20] V. Vo, M.N. Van, H.I. Lee, J.M. Kim, Y. Kim, S.J. Kim, A new route for obtaining Prussian blue nanoparticles, Mater. Chem. Phys. 107 (2008) 6–8. https://doi.org/10.1016/j.matchemphys.2007.07.002.
[21] C. Nie, X. Zhang, H. Ren, Z. Xing, X. Cao, J. Liu, D. Wei, Z. Ju, Synthesis of Manganese-Based Prussian Blue Nanocubes with Organic Solvent as High-Performance Anodes for Lithium-Ion Batteries, Eur. J. Inorg. Chem. 2019 (2019) 3277–3286. https://doi.org/10.1002/ejic.201900458.

[22] L. Hu, P. Zhang, Q. Chen, N. Yan, J. Mei, Prussian Blue Analogue Mn3[Co(CN)6]2·nH2O porous nanocubes: large-scale synthesis and their CO2 storage properties, Dalton Trans. 40 (2011) 5557–5562. https://doi.org/10.1039/C1DT10134J.
[23] K.K. Sand, J.D. Rodriguez-Blanco, E. Makovicky, L.G. Benning, S.L.S. Stipp, Crystallization of CaCO3 in Water–Alcohol Mixtures: Spherulitic Growth, Polymorph Stabilization, and Morphology Change, Cryst. Growth Des. 12 (2012) 842–853. https://doi.org/10.1021/cg2012342.
[24] D.B. Trushina, T.V. Bukreeva, M.N. Antipina, Size-Controlled Synthesis of Vaterite Calcium Carbonate by the Mixing Method: Aiming for Nanosized Particles, Cryst. Growth Des. 16 (2016) 1311–1319. https://doi.org/10.1021/acs.cgd.5b01422.
[25] J. Quinson, O. Aalling-Frederiksen, W.L. Dacayan, J.D. Bjerregaard, K.D. Jensen, M.R.V. Jørgensen, I. Kantor, D.R. Sørensen, L. Theil Kuhn, M.S. Johnson, M. Escudero-Escribano, S.B. Simonsen, K.M.Ø. Jensen, Surfactant-Free Colloidal Syntheses of Gold-Based Nanomaterials in Alkaline Water and Mono-alcohol Mixtures, Chem. Mater. 35 (2023) 2173–2190. https://doi.org/10.1021/acs.chemmater.3c00090.
[26] D. Parajuli, H. Tanaka, K. Sakurai, Y. Hakuta, T. Kawamoto, Thermal Decomposition Behavior of Prussian Blue in Various Conditions, Materials. 14 (2021). https://doi.org/10.3390/ma14051151.
[27] Z. Li, M. Dadsetan, J. Gao, S. Zhang, L. Cai, A. Naseri, M.E. Jimenez-Castaneda, T. Filley, J.T. Miller, M.J. Thomson, V.G. Pol, Revealing the Thermal Safety of Prussian Blue Cathode for Safer Nonaqueous Batteries, Adv. Energy Mater. 11 (2021) 2101764. https://doi.org/10.1002/aenm.202101764.
[28] K. Feng, J. Zhang, H. Dong, Z. Li, N. Gu, M. Ma, Y. Zhang, Prussian Blue Nanoparticles Having Various Sizes and Crystallinities for Multienzyme Catalysis and Magnetic Resonance Imaging, ACS Appl. Nano Mater. 4 (2021) 5176–5186. https://doi.org/10.1021/acsanm.1c00617.
[29] H. Bisswanger, Enzyme assays, Perspect. Sci. 1 (2014) 41–55. https://doi.org/10.1016/j.pisc.2014.02.005.
[30] B. Jiang, D. Duan, L. Gao, M. Zhou, K. Fan, Y. Tang, J. Xi, Y. Bi, Z. Tong, G.F. Gao, N. Xie, A. Tang, G. Nie, M. Liang, X. Yan, Standardized assays for determining the catalytic activity and kinetics of peroxidase-like nanozymes, Nat. Protoc. 13 (2018) 1506–1520. https://doi.org/10.1038/s41596-018-0001-1.
[31] T. Liu, D.R. Baek, J.S. Kim, S.-W. Joo, J.K. Lim, Green Synthesis of Silver Nanoparticles with Size Distribution Depending on Reducing

Species in Glycerol at Ambient pH and Temperatures, ACS Omega. 5 (2020) 16246–16254. https://doi.org/10.1021/acsomega.0c02066.
[32] P. Nalawade, T. Mukherjee, S. Kapoor, Green Synthesis of Gold Nanoparticles Using Glycerol as a Reducing Agent, Adv. Nanoparticles. 02 (2013) 78–86. https://doi.org/10.4236/anp.2013.22014.
[33] Z. Wang, H. Li, F. Tang, J. Ma, X. Zhou, A Facile Approach for the Preparation of Nano-size Zinc Oxide in Water/Glycerol with Extremely Concentrated Zinc Sources, Nanoscale Res. Lett. 13 (2018) 202. https://doi.org/10.1186/s11671-018-2616-0.
[34] P. Khramtsov, M. Kropaneva, A. Minin, M. Bochkova, V. Timganova, A. Maximov, A. Puzik, S. Zamorina, M. Rayev, Prussian Blue Nanozymes with Enhanced Catalytic Activity: Size Tuning and Application in ELISA-like Immunoassay, Nanomater. Basel Switz. 12 (2022) 1630. https://doi.org/10.3390/nano12101630.
[35] D.R. Rosseinsky, H. Lim, H. Jiang, J.W. Chai, Optical Charge-Transfer in Iron(III)hexacyanoferrate(II): Electro-intercalated Cations Induce Lattice-Energy-Dependent Ground-State Energies, Inorg. Chem. 42 (2003) 6015–6023. https://doi.org/10.1021/ic020575s.
[36] Y. Zhang, D. Kudriashov, L. Pershina, A. Offenhäusser, Y. Mourzina, Intrinsic Multienzyme-like Activities of the Nanoparticles of Mn and Fe Cyano-Bridged Assemblies, Nanomater. Basel Switz. 12 (2022) 2095. https://doi.org/10.3390/nano12122095.
[37] M.A. Komkova, K.R. Vetoshev, E.A. Andreev, A.A. Karyakin, Flow-electrochemical synthesis of Prussian Blue based nanozyme 'artificial peroxidase,' Dalton Trans. 50 (2021) 11385–11389. https://doi.org/10.1039/D1DT02107A.
[38] C. Shang, Q. Wang, H. Tan, S. Lu, S. Wang, Q. Zhang, L. Gu, J. Li, E. Wang, S. Guo, Defective PtRuTe As Nanozyme with Selectively Enhanced Peroxidase-like Activity, JACS Au. 2 (2022) 2453–2459. https://doi.org/10.1021/jacsau.2c00495.
[39] H. Yan, Y. Chen, L. Jiao, W. Gu, C. Zhu, Amorphous RuTe2 nanorods as efficient peroxidase mimics for colorimetric immunoassay, Sens. Actuators B Chem. 341 (2021) 130007. https://doi.org/10.1016/j.snb.2021.130007.
[40] R. Witter, M. Roming, C. Feldmann, A.S. Ulrich, Multilayered core–shell structure of polyol-stabilized calcium fluoride nanoparticles characterized by NMR, J. Colloid Interface Sci. 390 (2013) 250–257. https://doi.org/10.1016/j.jcis.2012.09.001.
[41] D.R. Handwerk, P.D. Shipman, C.B. Whitehead, S. Özkar, R.G. Finke, Mechanism-Enabled Population Balance Modeling of Particle Formation en Route to Particle Average Size and Size Distribution

Understanding and Control, J. Am. Chem. Soc. 141 (2019) 15827–15839. https://doi.org/10.1021/jacs.9b06364.
[42] X.-J. Zheng, Q. Kuang, T. Xu, Z.-Y. Jiang, S.-H. Zhang, Z.-X. Xie, R.-B. Huang, L.-S. Zheng, Growth of Prussian Blue Microcubes under a Hydrothermal Condition: Possible Nonclassical Crystallization by a Mesoscale Self-Assembly, J. Phys. Chem. C. 111 (2007) 4499–4502. https://doi.org/10.1021/jp065055n.
[43] J.B. Segur, H.E. Oberstar, Viscosity of Glycerol and Its Aqueous Solutions, Ind. Eng. Chem. 43 (1951) 2117–2120. https://doi.org/10.1021/ie50501a040.
[44] F.S. Jerome, J.T. Tseng, L.Tseng. Fan, Viscosities of aqueous glycol solutions, J. Chem. Eng. Data. 13 (1968) 496–496. https://doi.org/10.1021/je60039a010.
[45] Y. Tanaka, Y. Matsuda, H. Fujiwara, H. Kubota, T. Makita, Viscosity of (water + alcohol) mixtures under high pressure, Int. J. Thermophys. 8 (1987) 147–163. https://doi.org/10.1007/BF00515199.
[46] R.G. Walker, K.O. Watkins, Kinetics of complex formation between hexacyanoferrate(III) ions and iron(III) to form FeFe(CN)6 (Prussian brown), Inorg. Chem. 7 (1968) 885–888. https://doi.org/10.1021/ic50063a009.
[47] F. Shiba, U. Mameuda, S. Tatejima, Y. Okawa, Synthesis of uniform Prussian blue nanoparticles by a polyol process using a polyethylene glycol aqueous solution, RSC Adv. 9 (2019) 34589–34594. https://doi.org/10.1039/C9RA07080J.
[48] F. Fiévet, S. Ammar-Merah, R. Brayner, F. Chau, M. Giraud, F. Mammeri, J. Peron, J.-Y. Piquemal, L. Sicard, G. Viau, The polyol process: a unique method for easy access to metal nanoparticles with tailored sizes, shapes and compositions, Chem Soc Rev. 47 (2018) 5187–5233. https://doi.org/10.1039/C7CS00777A.
[49] H. Dong, Y.-C. Chen, C. Feldmann, Polyol synthesis of nanoparticles: status and options regarding metals, oxides, chalcogenides, and non-metal elements, Green Chem. 17 (2015) 4107–4132. https://doi.org/10.1039/C5GC00943J.
[50] S. Piana, F. Jones, J.D. Gale, Assisted Desolvation as a Key Kinetic Step for Crystal Growth, J. Am. Chem. Soc. 128 (2006) 13568–13574. https://doi.org/10.1021/ja064706q.
[51] X. Song, C. Dai, G. Chen, C. Dong, J. Yu, Effect of alcohol on the crystallization process of MgCO3·3H2O: an experimental and molecular dynamics simulation study, Energy Sources Part Recovery Util. Environ. Eff. 42 (2020) 1118–1131. https://doi.org/10.1080/15567036.2019.1602222.

[52] J.A. Cray, J.T. Russell, D.J. Timson, R.S. Singhal, J.E. Hallsworth, A universal measure of chaotropicity and kosmotropicity, Environ. Microbiol. 15 (2013) 287–296. https://doi.org/10.1111/1462-2920.12018.
[53] L. Catala, T. Mallah, Nanoparticles of Prussian blue analogs and related coordination polymers: From information storage to biomedical applications, Coord. Chem. Rev. 346 (2017) 32–61. https://doi.org/10.1016/j.ccr.2017.04.005.

Supplementary Information

To measure the pathlength for specific activity experiments, 180 µL of ponceau S dye solution in 10% DMSO was added to six wells of a 96-well plate. Subsequently, 20 µL of water was added to each well and quickly mixed, similar to the nanoparticle specific activity measurement procedure. Control wells were prepared by adding 20 µL of water to 180 µL of 10% DMSO. The absorbance at 513 nm was measured for both the dye solution and the control solution. Next, the dye solution from the wells was combined, and its absorbance at 513 nm was measured using a quartz cuvette with a 1 cm pathlength. The same procedure was carried out for the control solution. The pathlength for the wells was calculated as follows:

$$l_w = \frac{l_c \times (A_{dp} - A_{wp})}{(A_{dc} - A_{wc})}$$

where l_w is pathlength for plate wells, l_c is a pathlength of cuvette (1 cm), A_{dp} is an absorbance of dye solution in wells, A_{wp} is an absorbance of control solution in wells, A_{dc} is an absorbance of dye solution in cuvette, A_{wc} is the absorbance of the control solution in cuvette.

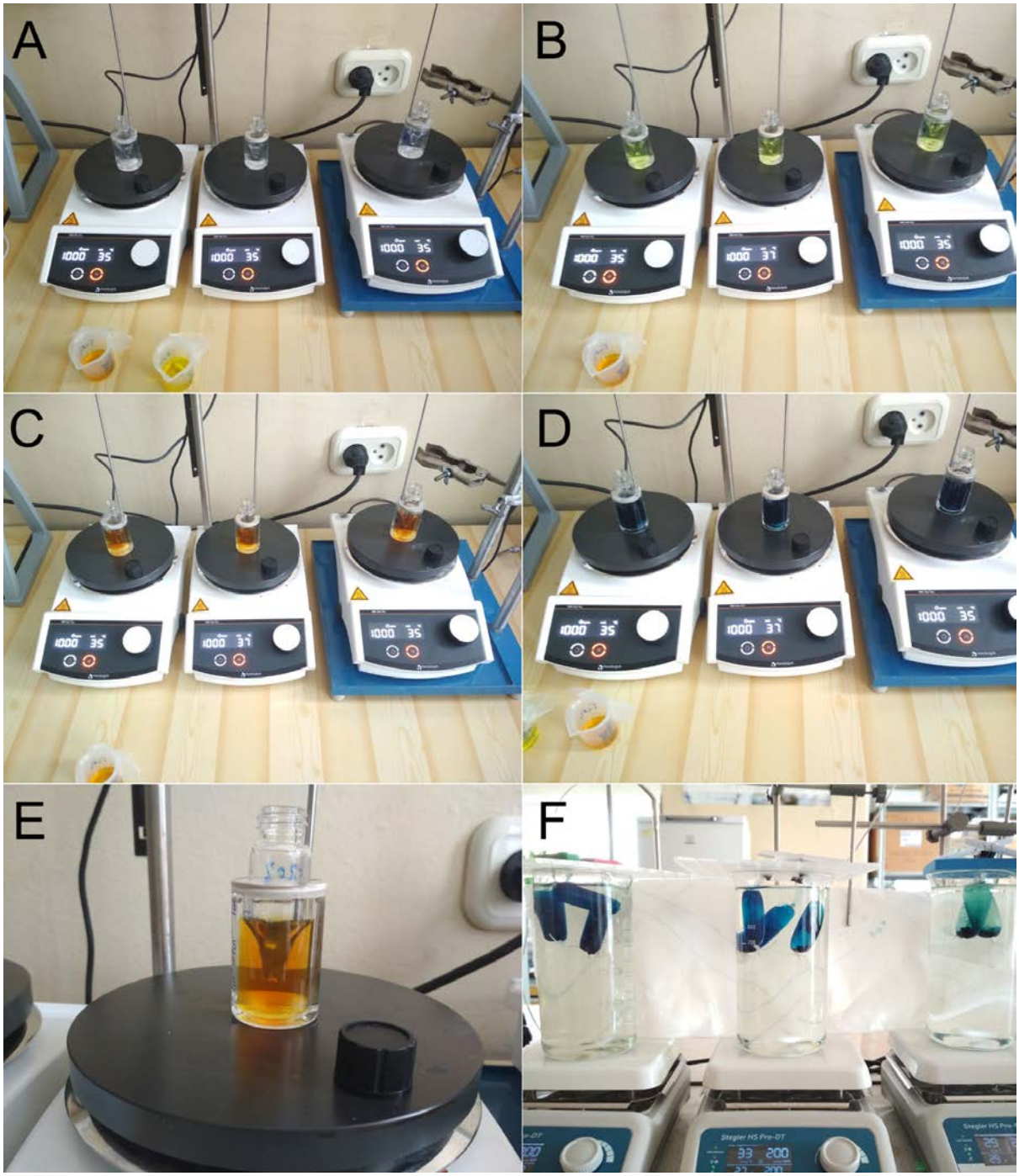

Fig. S1. Experimental setup of alcohol effect study. Vials with water/alcohol mixture (A), after the addition of $K_3[Fe(CN)_6]$ (B), after the addition of $FeCl_3$ (C), after the addition of H_2O_2 (D). Glass vial in the water bath (E). Dialysis of nanoparticles (F).

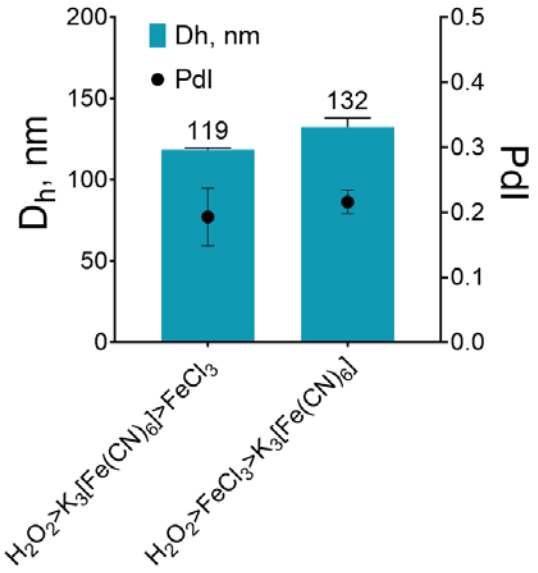

Fig. S2. Effect of reagent addition order. n=3, mean±SD.

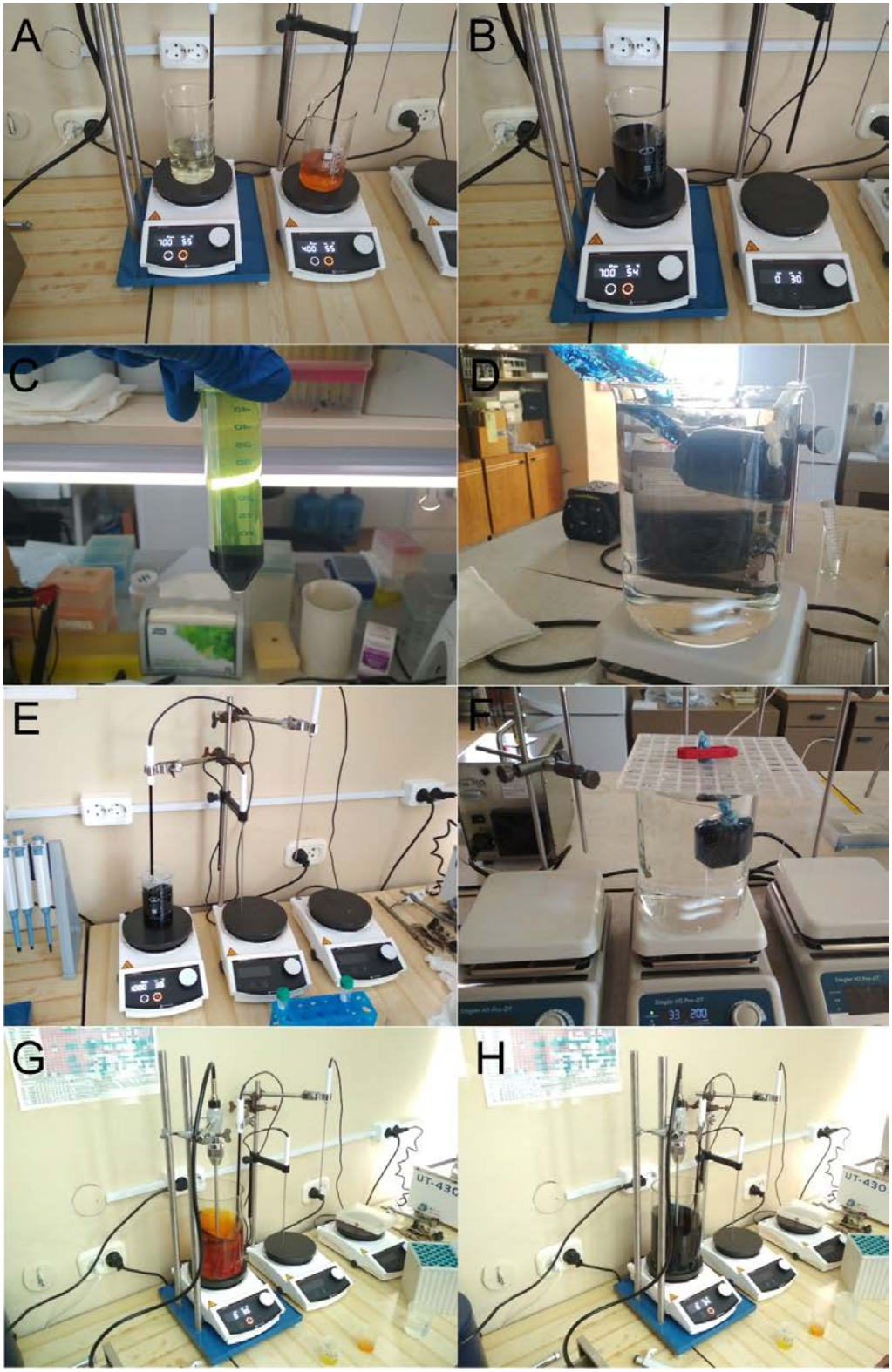

Fig. S3. Scaled-up synthesis of T-1 (A-D). Beakers with $K_4[Fe(CN)_6]$ and $FeCl_3$ before mixing (A) and after the mixing (B). Sediment of T-1 after centrifugation (C). Dialysis of T-1 (D). Scaled-up synthesis of EG-1 (E, F). Scaled-up synthesis of W-1 (E, F).

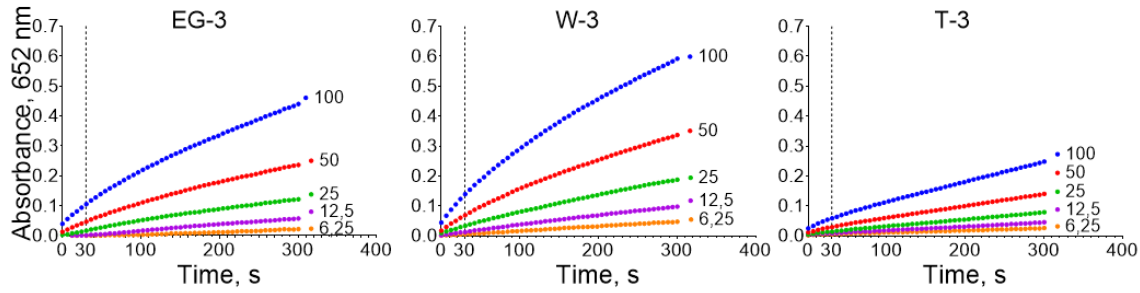

Fig. S4. Specific activity measurements of **EG-3**, **W-3**, and **T-3**. Absorbance vs time curves. Dashed line depicts the 30 s threshold of linear absorbance growth.

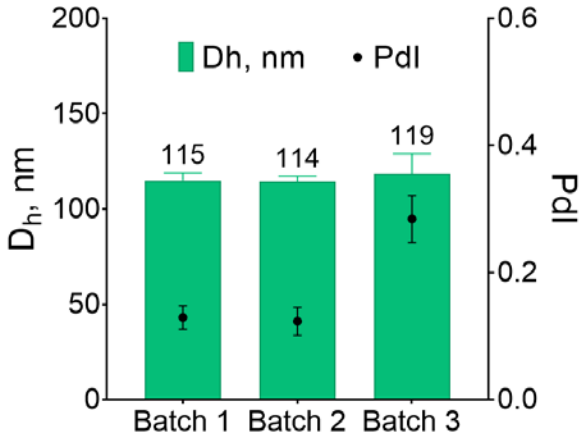

Fig. S5. Hydrodynamic diameter (D_h) and polydispersity (PdI) of nanoparticles synthesized in water, n=3, mean±SD.

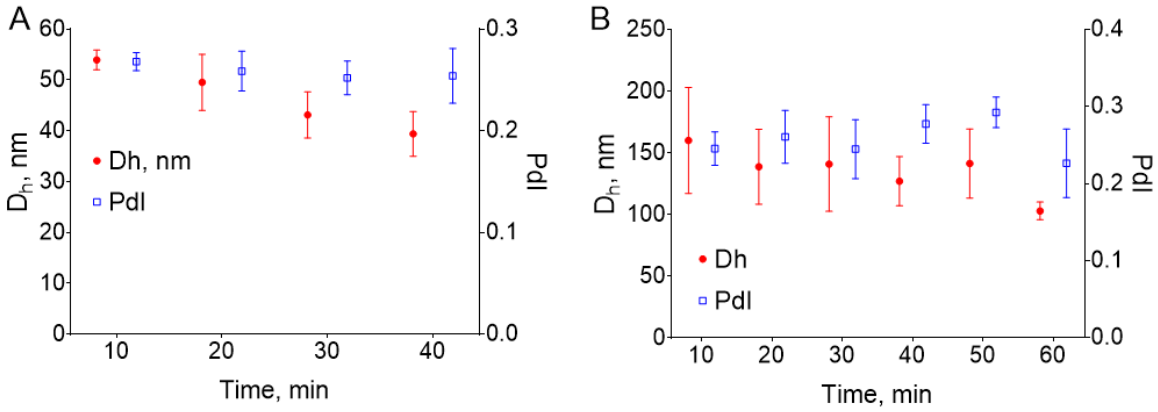

Fig. S6. Effect of sonication time on the size and polydispersity of nanoparticles in scale up experiment. Synthesis conditions: A - 79.2% ethylene glycol, 20 mM Fe salts, 140 mM H_2O_2, V=181 mL; B - H_2O, 3 mM Fe salts, 22 mM H_2O_2, V=909 mL, n=3, mean±SD.

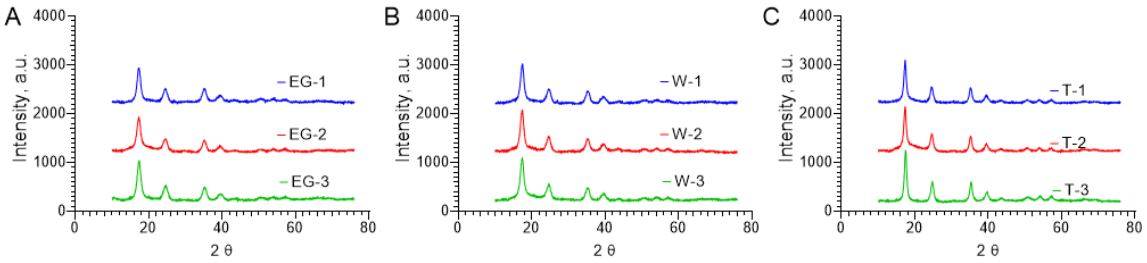

Fig. S7. XRD patterns of Prussian Blue nanoparticles

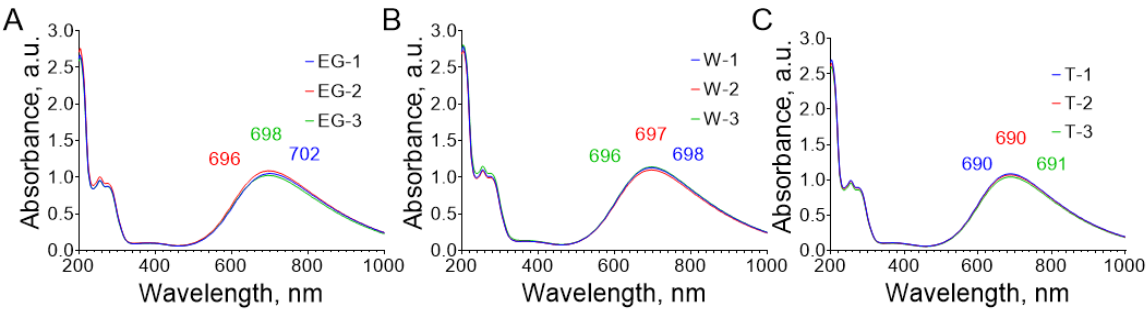

Fig. S8. UV-Vis spectra of Prussian Blue nanoparticles in deionized water. A - nanoparticles synthesized by reduction method in 79.2% ethylene glycol, B - in water, C - nanoparticles synthesized by the traditional method. Absorbance peaks for each spectrum are given. Concentration of nanoparticles - 40 μg/mL. Peak analysis was made in Origin software.

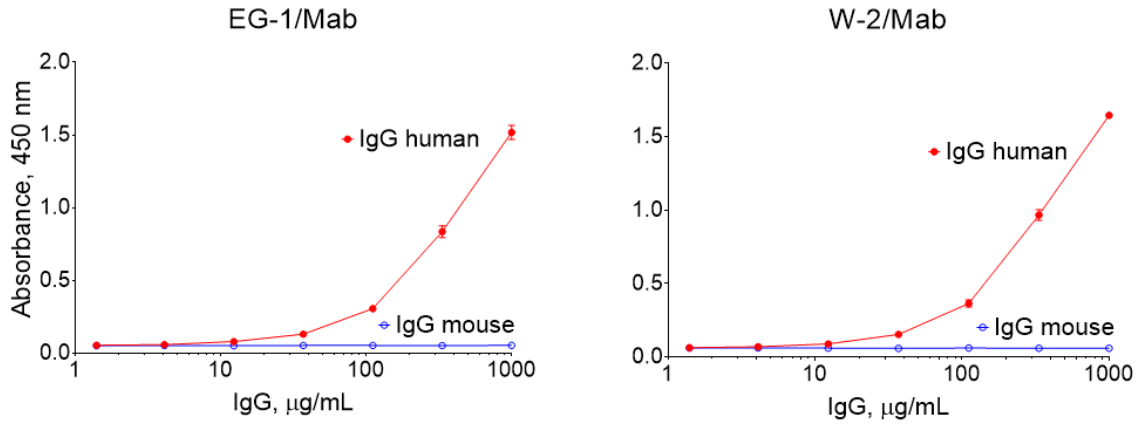

Fig. S9. Direct binding of EG-1/MAb and W-2/MAb with human and mouse IgG. n=3, mean±SD.

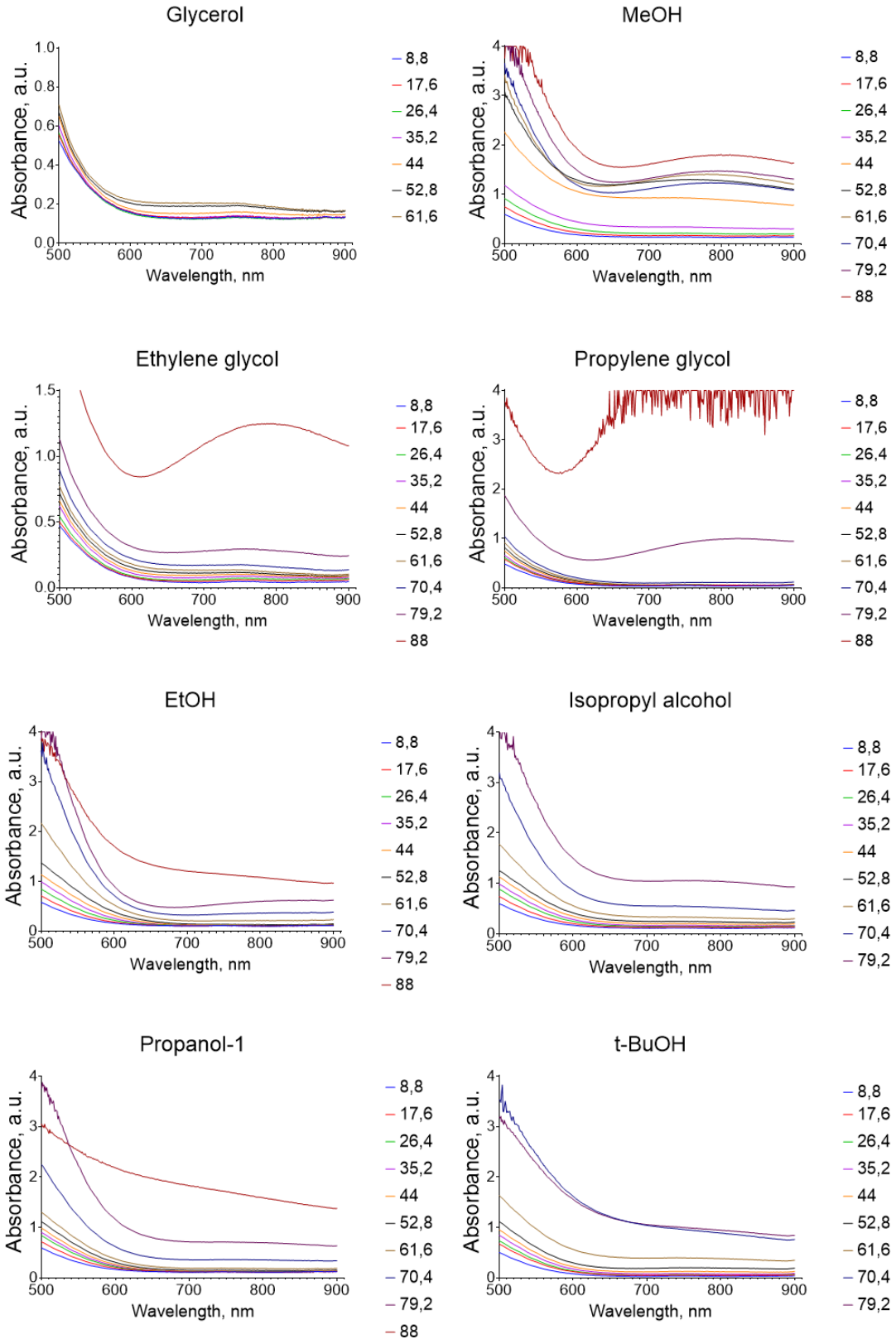

Fig. S10. Absorbance spectra of a 3 mm $FeCl_3/K_3[Fe(CN)]_6$ solution, taken 1 minute after adding the ferric salt to various water/alcohol mixtures (volume fractions are indicated to the right of the graphs).

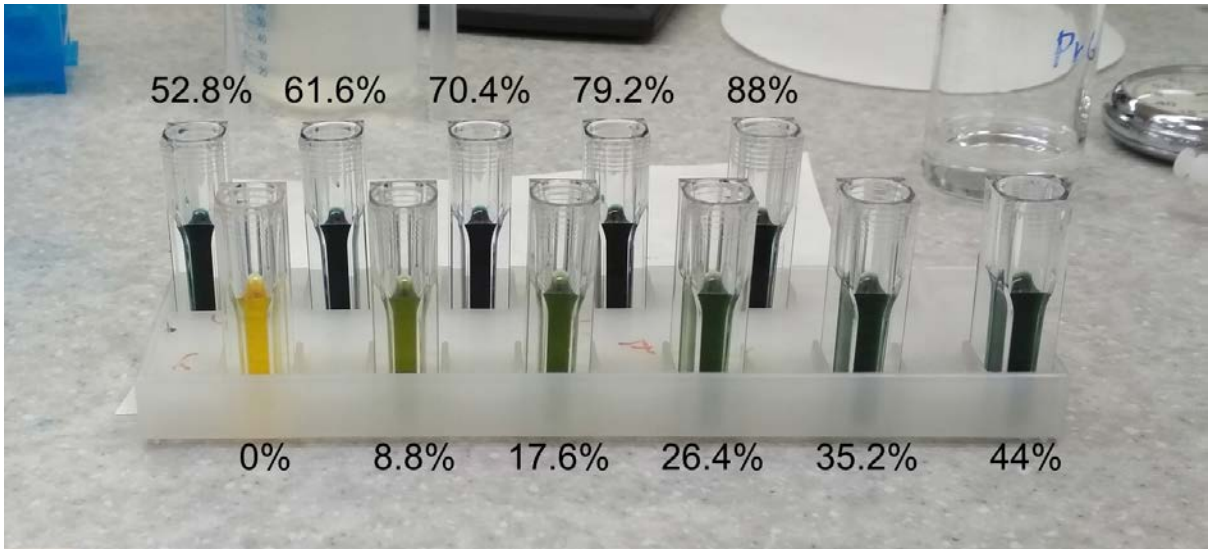

Fig. S11. Color of 3 mM $K_3[Fe(CN)_6]/FeCl_3$ in ethylene glycol-water mixtures. Volume fractions of ethylene glycol are given.

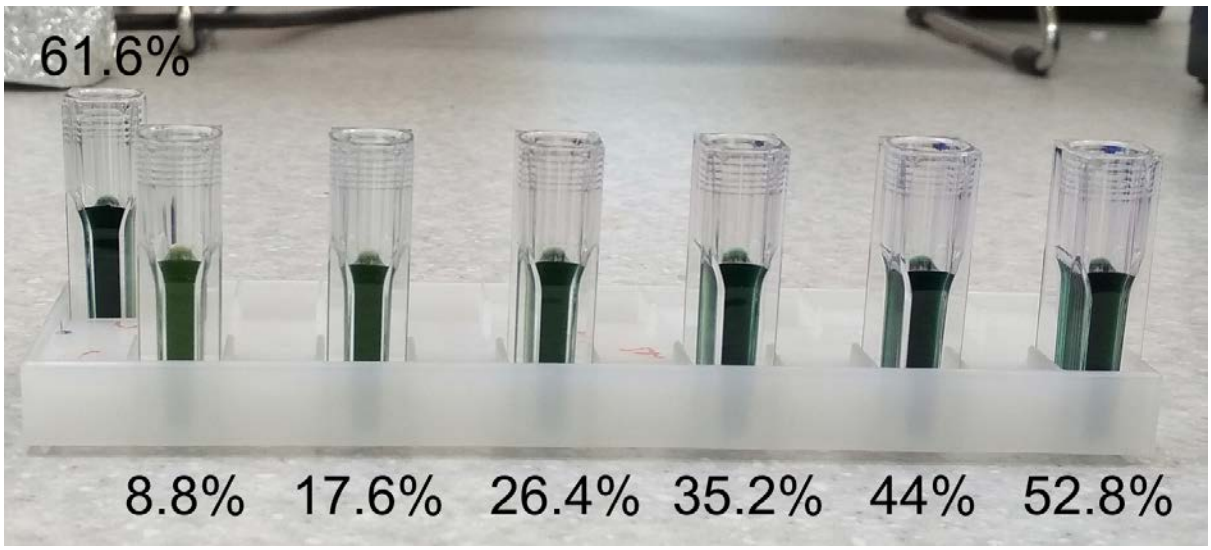

Fig. S12. Color of 3 mM $K_3[Fe(CN)_6]/FeCl_3$ in glycerol-water mixtures. Volume fractions of glycerol are given.

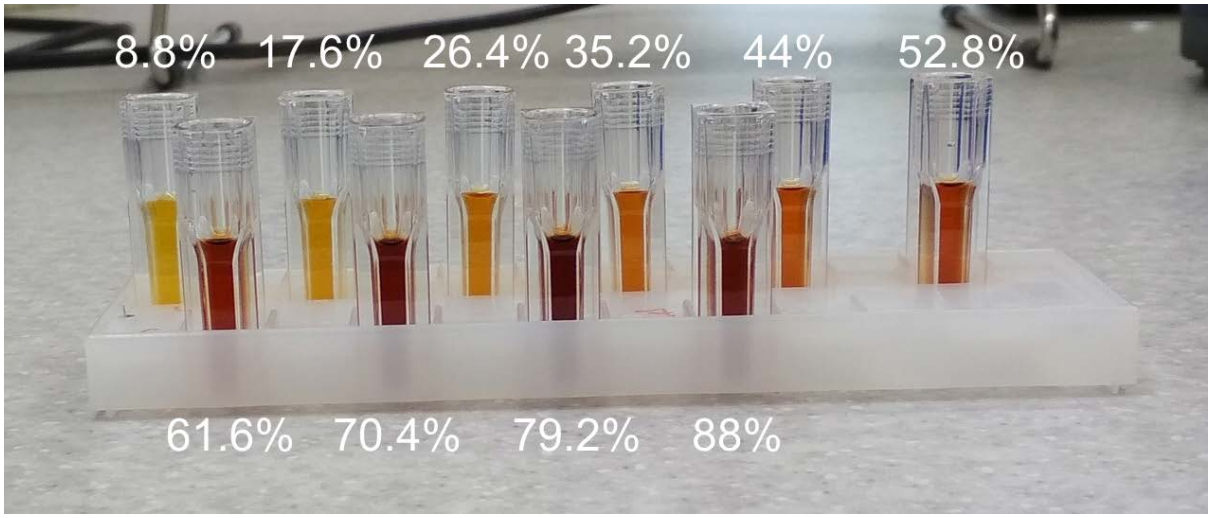

Fig. S13. Color of 3 mM $K_3[Fe(CN)_6]/FeCl_3$ in ethanol-water mixtures. Volume fractions of ethanol are given.

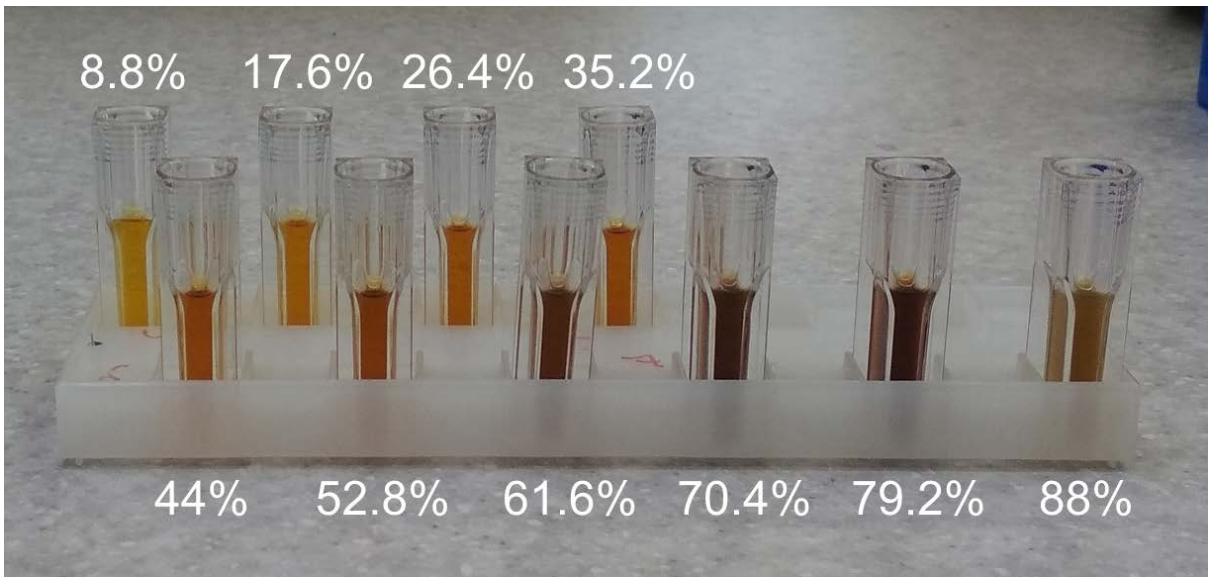

Fig. S14. Color of 3 mM $K_3[Fe(CN)_6]/FeCl_3$ in propanol-1-water mixtures. Volume fractions of propanol-1 are given.

Table S1. Size of nanoparticles before and after functionalization. n=3, mean±SD

	Dh, nm	PdI
EG-1	39.4±4.4	0.254±0.027
EG-1/MAb	43.9±0.3	0.210±0.003
W-2	128.2±30.6	0.285±0.081

W-2/MAb	133.1±33.3	0.273±0.090

Table S2. Dielectric constants of alcohols

Solvent	Glycerol	Ethylene glycol	Propylene glycol	Methanol	Ethanol	Propanol-1	Isopropyl alcohol	tert-butanol
ε	43	37.7	29.46	32.65	25.2	19.7	18.3	12.3